https://doi.org/10.5194/acp-2021-418
Preprint. Discussion started: 28 June 2021

Atmospheric Chemistry and Physics Discussions

15-year variability of desert dust optical depth on global and regional scales

Stavros-Andreas Logothetis[1], Vasileios Salamalikis[1], Antonis Gkikas[2] Stelios Kazadzis[3,4], Vassilis Amiridis[2] and Andreas Kazantzidis[1]

[1]Laboratory of Atmospheric Physics, Department of Physics, University of Patras, 26500 Patras, Greece
[2]Institute for Astronomy, Astrophysics, Space Applications and Remote Sensing, National Observatory of Athens, Athens, 15236, Greece
[3]Physics - Meteorology Observatory Davos, Word Radiation Center, Switzerland
[4]Institute of Environmental Research and Sustainable Development, National Observatory of Athens, Greece

Correspondence to: Andreas Kazantzidis (akaza@upatras.gr)

Abstract. This study aims to investigate the global, regional and seasonal temporal dust changes as well as the effect of dust particles on total aerosol loading, using the MIDAS fine resolution dataset. MIDAS delivers dust optical depth (DOD) at fine spatial resolution (0.1° x 0.1°) spanning from 2003 to 2017. Within this study period, the dust burden has been increased across Central Sahara (up to 0.023 yr^{-1}) and Arabian Peninsula (up to 0.024 yr^{-1}). Both regions observed their highest seasonal trends in summer (up to 0.031 yr^{-1}). On the other side, declining DOD trends are encountered in Western (down to −0.015 yr^{-1}) and Eastern (down to −0.023 yr^{-1}) Sahara, Bodélé Depression (down to −0.021 yr^{-1}), Thar (down to −0.017 yr^{-1}) and Gobi (down to −0.011 yr^{-1}) Deserts and Mediterranean Basin (down to −0.009 yr^{-1}). At spring, the most negative seasonal trends are recorded in Bodélé Depression (down to −0.038 yr^{-1}) and Gobi Desert (down to −0.023 yr^{-1}) whereas in West (down to −0.028 yr^{-1}) and East Sahara (down to −0.020 yr^{-1}), and Thar Desert (down to −0.047 yr^{-1}) at summer. Over western and eastern sector of Mediterranean Basin, the most negative seasonal trends are computed at summer (down to −0.010 yr^{-1}) and spring (down to −0.006 yr^{-1}), respectively. The effect of DOD to the total aerosol optical depth (AOD) changes is determined calculating the DOD to AOD ratio. Over Sahara Desert the median ratio values range from 0.83 to 0.95 whereas in other dust affected areas (Arabian Peninsula, South Mediterranean, Thar and Gobi Deserts) is recorded approximately around 0.6. In addition, a comprehensive analysis of the factors effecting the sign, the magnitude and the statistical significance of the calculated trends is conducted. Firstly, the implications between the implementation of geometric mean instead of arithmetic mean to trend calculations are discussed revealing that the arithmetic-based trends tend to overestimate compared with the geometric-based trends both over land and ocean. Secondly, an analysis interpreting the differences in trend calculations under different spatial resolutions (fine and coarse) and time intervals is conducted, which sounds a critical aspect when satellite-based measurements are utilized.

https://doi.org/10.5194/acp-2021-418
Preprint. Discussion started: 28 June 2021

Atmospheric Chemistry and Physics Discussions

1 Introduction

Dust particles emitted from natural or anthropogenic sources constitute the major contributor of the atmospheric aerosol burden in terms of mass (Zender et al. 2004; Textor et al., 2006; Kok et al., 2017). Among aerosol properties, aerosol optical depth (AOD) describes adequately aerosols' load, in optical terms, corresponding to the entire atmospheric column. The proportion of AOD attributed to dust particles consists the dust optical depth (DOD). The spatiotemporal patterns of mineral particles are determined by the components of the dust life cycle characterized by a pronounced heterogeneity (Mahowald et al., 2014). The main natural dust sources are located in the northern hemisphere (Goudie and Middleton., 2006), with Sahara region being the most dominant one (Prospero et al., 2002; Goudie and Middleton, 2006; Rajot et al., 2008; Alizadeh-Choobari et al., 2014a). Other active source areas of mineral particles are situated in the Middle East and the region stretching from Mesopotamia to the Oman coasts in south Arabian Peninsula (Prospero et al., 2002; Ginoux et al., 2012), in southwest Asia and Sistan Basin (Iran-Pakistan-Afghanistan) (Alizadeh-Choobari et al., 2014b; Rashki et al., 2015), in Central Asia across the Karakum (Turkmenistan-Uzbekinstan) and Kyzylkum Deserts (southeast of the Aral sea in Uzbekistan) (Elguindi et al., 2016), in East Asia with Taklamakan (Tarim basin in northwest China) and Gobi (north China – south Mongolia) deserts (Ginoux et al., 2012), and in North America with Black Rock and Smoke, Great Salt Lake, and Chihuahuan and Sononan deserts (Ginoux et al., 2012).

Mineral dust aerosols are uplifted, accumulated into the atmosphere, and transported over enormous distances (up to some thousands of kilometers) from their sources (Goudie and Middleton., 2006) driven by the prevailing winds. Schepanski et al. (2018) reported that the transport distance of dust particles is strongly related to their residence time, which is analogous to the dust lifetime, dust layer altitude, atmospheric circulation pattern, buoyancy and gravitational forces. van der Does et al. (2018) also denoted that strong winds, turbulence, electrostatic forces developed by dust particles' charging, and thunderstorms or tropical cyclones may potentially enhance the residence time of dust aerosols into the atmosphere. On a seasonal basis, dust particles can be transported from north Africa towards to the Atlantic Ocean reaching Caribbean, Central America, southern United States (in boreal summer) and south America (in spring and winter) (Griffin et al., 2002; Prospero and Lamb., 2003; Kalashnikova et al., 2008; Huang et al., 2010; Tsamalis et al., 2013; Prospero and Mayol-Bracero., 2013). Additionally, Saharan dust is advected towards the Mediterranean and Europe (Mona et al., 2006; 2012, Papayannis et al., 2008; Basart et al., 2009; Schepanski et al., 2018; Gkikas et al. 2015; 2016, Logothetis et al., 2020, 2021).

During the last decades, numerous studies have been conducted using observations from various satellite sensors. Prospero et al. (2002) and Ginoux et al. (2012) identified the global dust sources relying on Total Ozone Mapping Spectrometer (TOMS, Torres et al., 2002) and Moderate Resolution Imaging Spectroradiometer (MODIS, Remer et al., 2008), respectively. More specifically, the studies of Prospero et al. (2002) and Ginoux et al. (2012) were based on the frequency of occurrence (FoO) of TOMS absorbing aerosol index (AAI) and MODIS-based DOD, respectively, exceeding defined thresholds. In addition, Ginoux et al. (2012) associated the dust frequency with three clusters such as hydrologic and non-hydrologic natural or anthropogenic in order to distinguish the dust origin. Similarly, at a regional scale, Schepanski et al. (2012) implemented a

https://doi.org/10.5194/acp-2021-418
Preprint. Discussion started: 28 June 2021

comprehensive analysis on the potential differences of Saharan dust active sources within the intercomparison of aerosol properties observations derived from MODIS, Meteosat Second Generation (MSG) and Ozone Monitoring Instruments (OMI). Voss and Evan (2020) presented a global DOD climatology, both over land and ocean, using MODIS (Aqua and Terra) from 2001 to 2018 and Advanced Very High Resolution Radiometer (AVHRR) over ocean from 1981 to 2018. Similarly, Clarisse et al. (2019) performed a global seasonal DOD climatology relying on Infrared Atmospheric Sounding Interferometer (IASI) retrievals, during the 2008-2017. Yu et al. (2019), derived DOD using MODIS, IASI and Multiangle Imaging Spectroradiometer (MISR) and in conjunction with dust vertical profiles from Cloud−Aerosol Lidar with Orthogonal Polarization (CALIOP) (Shikwambana and Sivakumar., 2018) investigated the dust deposition and loss frequency across the Tropical Atlantic Ocean on a seasonal basis.

The investigation of dust loads' variation at interannual time scales is quite critical for assessing the associated impacts on climate as well as the response of these tendencies to environmental factors. Since the majority of remote sensing instruments provide an AOD product, numerous studies on a global scale, are focused on the estimation of AOD temporal trends, which are not always representative of DOD, being mixed with other aerosol types (Zhang and Reid, 2010; de Meij et al., 2012; Hsu et al., 2012; Yoon et al., 2014; Pozzer et al., 2015; Alfaro-Contreras et al., 2017; Zhao et al., 2017; Che et al., 2019) and regional scales (Guo et al., 2011; Li, 2014; Klingmüller et al., 2016; Floutsi et al., 2016; Dahutia et al., 2017; Hu et al., 2018; Zhang et al., 2018). Limited satellite studies are dedicated to the estimation of DOD temporal trends due to the deficiency to quantify accurately the portion of AOD attributed to DOD. Prior studies have investigated the interannual patterns of DOD, both in sign and magnitude, over the "dusty" regions of the planet. Dust load has been increased across the Sahara Desert (Voss and Evan 2020), based on MODIS-Aqua derived DOD dataset during 2003-2018. Notaro et al. (2015) detected a regime shift in dust activity between 1998-2005 (inactive dust period) and 2007-2013 (active dust period) across Arabian Peninsula, which is attributed to the prolonged drought along the Fertile Crescent. Through the synergy of MISR DODs and back trajectories, they revealed that the positive DOD anomalies (increased dust burden) are strongly connected with dust advection from the Fertile Crescent towards the Arabian Peninsula. These findings are consistent with the strong positive AOD (Klingmüller et al., 2016) and DOD (Voss and Evan 2020) trends reported in the area. Voss and Evan (2020), found a reduction of dust load across the Northern African coasts over the period 2001-2018, based on MODIS-Terra DOD dataset. Declining DOD trends have also been reported in Central Asia by Xi and Sokolik (2015), who analyzed MODIS and Sea-viewing Wide Field-of-view Sensor (SeaWiFs) DODs for a 15-year period (2000-2014). DOD trend sign is also abruptly changed from positive (1999-2009) to negative (2010-2016) over East Asia and North Pacific Ocean in springtime, based on Modern-Era Retrospective Analysis for Research and Applications, Version 2 (MERRA-2) (Gelaro et al., 2017) measurements (Guo et al., 2019). Across South Asia, a negative shift in DOD interannual variation is recorded during the pre-monsoon season between 2008-2012 and 2013-2017, based on CALIOP observations (Lakshmi et al., 2019). In the southern sector of the Gobi Desert, declining DOD trends are observed from MODIS and CALIOP DOD datasets during 2007-2019 (Song et al., 2021).

A few aspects regarding the key points of the current study are highlighted in order to support its novelty as well as the scientific contribution of this study to the relevant research field. In contrast to the existing studies, this analysis relies on fine

https://doi.org/10.5194/acp-2021-418
Preprint. Discussion started: 28 June 2021

spatial resolution data thus making feasible to depict in detail the spatial patterns of the dust optical depth trends. Such information can be critical for the interpretation of the perturbations of the radiation fields, environmental impacts and health effects attributed to dust. One more advantage of the high resolution DOD analysis is the flexibility on the final grid size selection depending on data availability, a critical aspect when satellite observations are used. MIDAS data can be easily upscaled at coarser spatial resolutions in order to match spaceborne observations which have been commonly used in trend analyses available in literature (Hsu et al., 2012; Yoon et al., 2014; Notaro et al., 2015; Pozzer et al., 2015; Klingmüller et al., 2016; Alfaro-Contreras et al., 2017; Che et al., 2019; Guo et al., 2019; Voss and Evan 2020; Song et al., 2021). Nevertheless, relying on fine spatial resolution data it is ensured a more realistic collocation with ground-based measurements for validating the obtained DOD trends. Another interesting point is that few studies have concentrated on pure DOD (Xi and Sokolik 2015; Guo et al., 2019; Lakshmi et al., 2019; Voss and Evan 2020; Song et al., 2021) rather than AOD to analyze trends of mineral particles' load. Even though the consideration of the latter parameter is quite reasonable across deserts, its representativeness over downwind areas it is questionable due to the coexistence of other aerosol types. Such types can play a role also on DOD trend uncertainty. In MIDAS, this issue is addressed by adjusting the MODIS AOD to DOD via the consideration of the MERRA-2 dust fraction whereas in other studies, aerosol size and natural optical properties, which their quality above land is downgraded, are used in parallel. Taking advantage that MIDAS provides DOD and quality assured AOD, their trends are discussed jointly for assessing the contribution of dust burden temporal variations to those of the total aerosol load. Also, this is the first study assessing the effect of DOD to total AOD trends across the major desert dust areas of the planet, highlighting the crucial role of desert dust particles in past, present and future AOD trend studies. Another innovative element here is the investigation of the potential impact on trends' magnitude, sign and statistical significance when different DOD aggregations (i.e., arithmetic mean vs. geometric mean) are considered among various spatial and temporal scales. In addition, the DOD interannual variations are discussed not only for the entire study period, but also on a seasonal basis as well as for sub-periods, trying to identify alternations on DOD trends within the period of interest. This is done not only at global scale but also for key regions of the planet encompassing the major dust sources and downwind areas. For the sake of clarity, it must be noted that most of the aforementioned points have been already analyzed in previous studies but not in a common context as it is performed here.

The main objective of this work is the investigation of dust temporal variations, both at global and regional scale, using the MIDAS DOD product over the period 2003-2017. Sect. 2 describes (i) the MIDAS dataset (Sect. 2.1) and (ii) the trend detection methodology (Sect. 2.2). The results section (Sect. 3) is divided into three sub-sections analyzing (i) the global AOD and DOD tendencies, along with three sensitivity analyses between fine (0.1° x 0.1°) and coarse (1° x 1°) spatial resolutions, arithmetic and geometric means and filtered and non-filtered data trend calculations (Sect. 3.1), (ii) global dust temporal trends on a seasonal basis (Sect. 3.2), and (iii) DOD temporal tendencies into specific regions (Sect. 3.3). Finally, a discussion focusing on the main findings of this study is presented in the summary and conclusion section (Sect. 4). The current study represents a practical implementation of the MIDAS dataset and aims to demonstrate its feasibility on the estimation of dust load variation at various temporal and spatial scales.

https://doi.org/10.5194/acp-2021-418
Preprint. Discussion started: 28 June 2021

2 Data and Methods

2.1 Modis Dust AeroSol (MIDAS) dataset

MIDAS dataset (Gkikas et al., 2021) provides columnar DOD at 550 nm, on a daily basis over the 15-year period spanning from 2003 to 2017, at a global scale and fine spatial resolution (0.1° x 0.1°). Its development has relied on the synergistic implementation of quality filtered AOD retrievals from MODIS-Aqua (Level 2; Collection 6.1) and MERRA-2 dust fraction (MDF), both reported at 550 nm. More specifically, the multiplication of MODIS-Aqua AOD with MDF provides the MIDAS-DOD on MODIS native grid which is converted to an equidistant lat-lon projection. In order to justify the reliability of MDF, it has been evaluated against the corresponding portion provided by the LIVAS database (Amiridis et al., 2013; Amiridis et al., 2015). Based on the aforementioned assessment analysis, it has been revealed an adequate representation of MERRA-2 dust fraction, in optical terms, over the main dust sources and the outflow regions, in contrast to areas where dust presence is weak. Therefore, the combination of highly accurate MODIS AODs and quite reliable MDF results in a trustworthy MIDAS DOD product. This has been justified via its evaluation against AERONET AODs and its intercomparison versus DOD derived by LIVAS and MERRA-2. For the former analysis, the ground-based AODs have been treated appropriately in order to resemble DOD, as much as possible, assuming that the contribution of fine mineral particles is negligible and trying to minimize the contribution of non-dust aerosol species to the columnar aerosol load. Under these assumptions, the evaluation metrics, both at global and station level, reveal a quite high level of agreement between the two datasets. At global scale, there is a high level of agreement between MIDAS and AERONET DODs as indicated by the high correlation (~0.9) and the low positive bias (0.004 or 2.7%). Across the 'dust belt', the correlation coefficients can reach up to 0.98 at station level whereas positive biases (mostly lower than 0.06) are found. Outside of this zone, the correlation reduces, and the biases of similar magnitude are switching to negative. Likewise, it has been evident a considerable consistency among MIDAS, LIVAS and MERRA-2 DODs at global and hemispherical scales, despite the different approaches applied for the DOD derivation, whereas the intercomparison results are regionally dependent. Summarizing, in Gkikas et al. (2021) it has been justified the reliability of the MIDAS DOD thus allowing its utilization for investigating the temporal trends of dust aerosol burden over long-time periods and at various spatial scales.

2.2 Temporal trends methodology

The spatiotemporal changes of dust particles' burden, over the period 2003 – 2017, are investigated by calculating the annual trends derived by the monthly MIDAS DODs. At each grid-cell, the monthly DOD averages are calculated when the 20% (≥ 6 days) of daily data are available (Hsu et al., 2012). Subsequently, at the grid points with more than 60 months available (5 out of 15 complete years) linear trends are calculated by the implementation of the following equation,

$$Y_t = \mu + S_t + \omega X_t + N_t \tag{1}$$

https://doi.org/10.5194/acp-2021-418
Preprint. Discussion started: 28 June 2021

where Y_t is the monthly averaged values, μ the offset term, S_t is the seasonal term (long-term monthly value), ω the linear trend and N_t the residuals. The seasonality is removed by subtracting S_t from Y_t. The statistical significance of ω is derived according to Weatherhead et al. (1998). N_t follows a 1st-order autoregressive process (significant lag-1 autocorrelation),

$$N_t = \varphi N_{t-1} + \varepsilon_t \tag{2}$$

with ε_t is the white noise and φ the lag-1 autocorrelation coefficient. The standard deviation of the trend can be expressed as,

$$\sigma_\omega \approx \frac{\sigma_N}{n^{3/2}}\sqrt{\frac{1+\varphi}{1-\varphi}} \tag{3}$$

where σ_N is the standard deviation of N_t and n is the number of complete years depending on the data availability at each grid cell without always considering the entire period (i.e., a constant value of 15 years). When $|\omega/\sigma_\omega|>2$, significant temporal trends are considered at a 95% confidence level. The methodology of Weatherhead et al. (1998) is commonly applied in numerous studies concerning the detection of temporal trends in AOD (Hsu et al., 2012; Babu et al., 2013; Li et al., 2014; Kumar et al., 2015, 2018; Pozzer et al., 2015; Adesina et al., 2016; Alfaro-Contreras et al., 2017; Zhang et al., 2018; Ningombam et al., 2019). Additionally, for comparison purposes with previous studies, AOD and DOD linear trends are calculated also at 1° spatial resolution. The re-gridding procedure from fine to coarse spatial resolution is implemented following Levy et al. (2009) (upper branch in Fig. 5 of their publication). For the calculation of regional trends (Sect. 3.3), the same approach is adopted. First, daily spatial grids of 0.1° are temporally averaged to create monthly data. Then, monthly grids with 1° spatial resolutions are generated using a weighted aggregation of monthly fine grids. The weighting factors are defined in terms of latitude. More specifically, this weighting scheme considers the fraction between the area covered by each fine grid-cell to the total available surface area within the coarse grid-cell.

The appropriate selection of the statistical average metric (e.g. arithmetic mean) is reflected to the background probability distribution which the raw data are resembled. For instance, the vast majority of the studies focusing on AOD statistics have thoroughly consider that AOD follows a Gaussian distribution using the simple arithmetic mean for temporal and spatial aggregations. Nevertheless, the frequency distribution of AOD follows in general the log-normal distribution (O' Neill et al., 2000). Sayer and Knobelspiesse (2019) designated that the calculation of the geometric instead of the arithmetic mean for obtaining temporal and spatial AOD trends may overestimate them comparing to those reported in the literature. Here, in order to investigate the potential differences on AOD and DOD temporal trends, a sensitivity analysis using both geometric and arithmetic mean is established. MIDAS dataset includes negative DOD values introduced from the applied Dark Target algorithm of MODIS AOD retrievals. Since negative arguments of logarithm cannot be defined, all these negative values are overwritten to 0.0001 as suggested by Sayer and Knobelspiesse (2019).

https://doi.org/10.5194/acp-2021-418
Preprint. Discussion started: 28 June 2021

3 Results

This section is divided into three main parts. Sect. 3.1 describes the geographical distribution of AOD and DOD trends, both for fine and coarse AODs/DODs at global scale. In addition, sensitivity analysis for the spatial resolution (fine vs. coarse), aggregation metric (geometric vs. arithmetic mean), and temporal criteria (filters vs no filters) is performed. In Sect. 3.2, focus is given on the seasonal DOD trends whereas in Sect 3.3 emphasis is given on DOD trends at 12 regions of interest.

3.1 Global trends

Along with the detection of global AOD/DOD trends, a sensitivity analysis on (Sect. 3.1.1) geometric vs. arithmetic mean, (Sect. 3.1.2) fine vs. coarse spatial resolution and (Sect. 3.1.3) filtered vs. non-filtered for AOD/DOD trend calculations is presented.

3.1.1 Geometric vs. arithmetic mean

The first sensitivity analysis of this section deals with the potential differences in AOD and DOD trend calculations using geometric (log-normal distribution) rather than arithmetic mean (normal distribution) for satellite-based observations. Sayer and Knobelspiesse (2019) used AOD at three AERONET stations located in North America (Goddard Space Flight Center, GSFC), Arabian Peninsula (Solar Village) and over ocean (Ascension Island) for the calculation of the decadal AOD trends using arithmetic and geometric means for the monthly and seasonal averaged values. The sign of AOD trends for both aggregation metrics was found identical. Nevertheless, the arithmetic-based trends were higher in absolute terms comparing to the geometric-based ones, highlighting the significance in the selection of temporal aggregation metric in trend calculations. Based on sensitivity analysis (not shown here) of MIDAS climatological DOD means, differences between arithmetic and geometric mean are revealed, confirming that DODs population fits better a log-normal distribution. The latter considers the extreme dust episodes which force the distribution curve to be right-skewed (log-normal distribution curve). In this study, all AOD and DOD trends are observed similar in sign either for fine (Fig. 1) or coarse (Fig. S1) spatial resolution. However, quantitatively differences are revealed between arithmetic and geometric trends. When geometric AOD/DOD averages are considered, the deseasonalized trends are suppressed with the respect to the corresponding levels obtained from the arithmetic means both over continental (from 68.33 to 82.60%) (Fig. S2) and maritime (from 52.87 to 91.77%) (Fig. S3) areas, except for AOD trends at 1° spatial resolution (28.37%) (Fig. S3c). This is expected based on the fact that geometric means are lower than averages.

https://doi.org/10.5194/acp-2021-418
Preprint. Discussion started: 28 June 2021

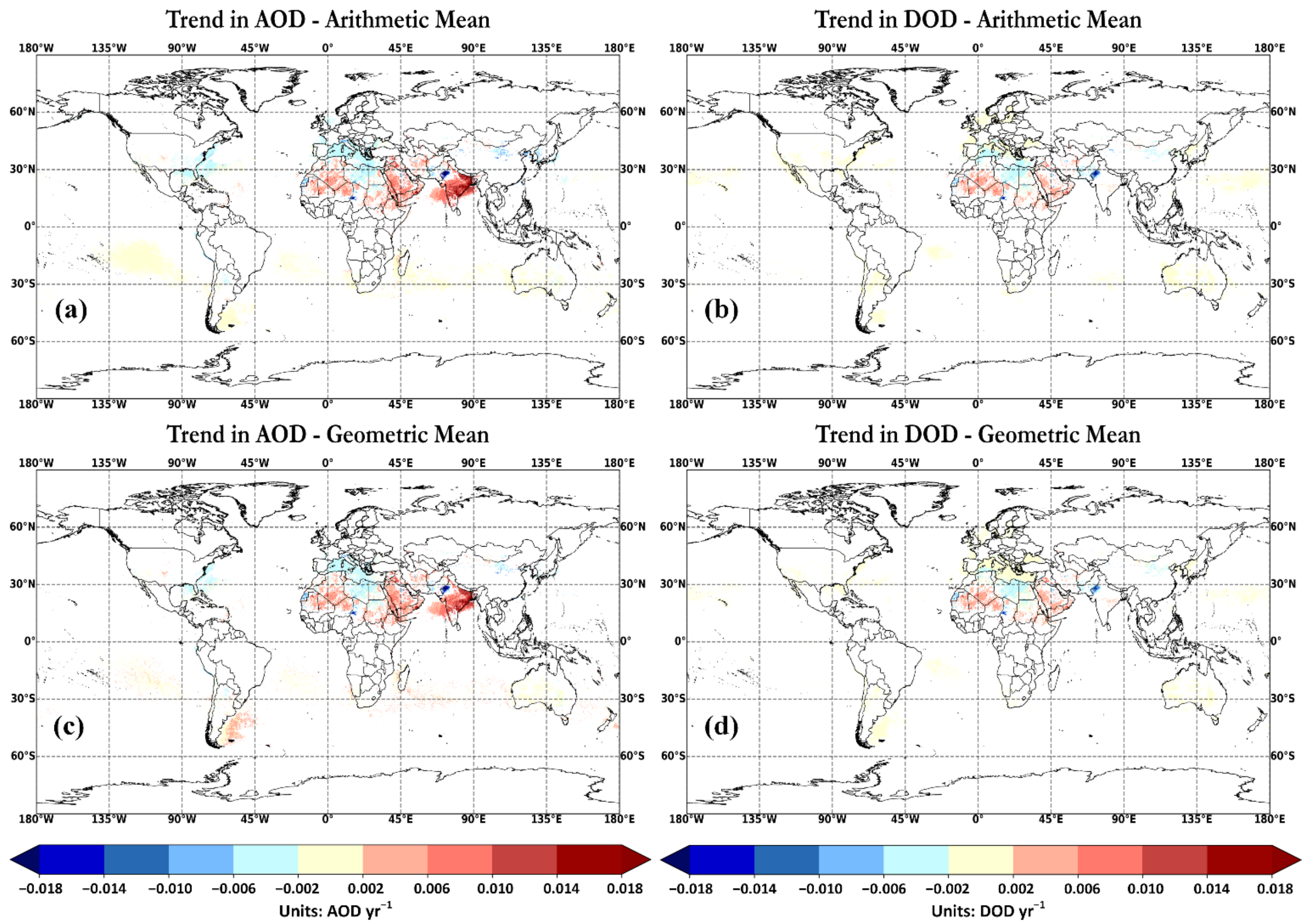

Figure 1: Global maps of temporal trends (significant under the 95% confidence level), at 0.1° x 0.1° spatial resolution, calculated from the deseasonalized AOD (a and c) and DOD (b and d) monthly values during 2003 – 2017. Upper panel (a, b) shows the arithmetic-based trends while the bottom panel (c, d) indicates the geometric-based trends.

At fine spatial resolution, statistically significant annual AOD and DOD trends are recorded in specific regions of the planet (Fig. 1). The patterns of AOD and DOD trends reveal many similarities in most regions. Over areas where the dust contribution to the total aerosol load is negligible, DOD trends are non-significant or neutral (blank or yellow cells in Figs. 1b and 1d). For instance, strong positive AOD trends are depicted across India and Bay of Bengal (Figs. 1a and 1c), whereas the recorded annual DOD tendencies are negligible (Figs. 1b and 1d). Similar findings are evident along the eastern coasts of US and in the Gulf of Mexico. Regarding the Mediterranean Basin, engrossing disparities are recorded between AOD and DOD trends. Negative AOD trends are shown in the entire region with decreasing DOD trends confined in the southern areas near the North Africa coast (Figs. 1b and d). Strong positive trends for AOD and DOD are revealed in Central Sahara (up to 0.026 yr^{-1}), across Mauritania-Algeria-Mali-Niger areas and the Arabian Peninsula. The highest positive tendencies are shown in Oman−Saudi Arabia border (up to 0.031 yr^{-1}). On the contrary, decreasing AOD/DOD tendencies are observed in the Eastern

https://doi.org/10.5194/acp-2021-418
Preprint. Discussion started: 28 June 2021

(down to −0.017 yr^{-1}) and Western (down to −0.019 yr^{-1}) Sahara, in the Bodélé Depression of the Chad Basin (northern of Lake Chad), in the Gobi Desert (Northern China−Southern Mongolia) as well as in the Thar Desert (northwestern Indian subcontinent). Among the regions where declining tendencies are evident, the most negative ones are recorded in the Bodélé Depression (down to −0.025 yr^{-1}) and in the Thar Desert (down to −0.029 yr^{-1}). A comprehensive regional analysis including the intercomparison with prior findings and the potential trends justification is discussed in Sect. 3.3.

3.1.2 Fine vs. coarse spatial resolution

The second sensitivity analysis aims to highlight differences of AOD/DOD trends when fine and coarse spatial resolution of MIDAS data are contrasted. A similar study made by de Meij et al. (2012), shows a good agreement between MODIS daily L2 and monthly L3 dataset over specific areas (i.e., Central Mediterranean, North-East America, and East Asia). At a first glance, the trend patterns reproduced by the fine (Fig. 1) and coarse (Fig. S1) MIDAS DODs are spatially consistent. Nevertheless, in terms of magnitude, the absolute values of DODs at coarser spatial resolution are lower in most of areas with evident signal (either positive or negative), such as the southern parts of the Arabian Peninsula (up to 0.014 yr^{-1}), the Bodélé Depression (down to −0.015 yr^{-1}) and the Thar Desert (down to −0.024 yr^{-1}). On a regional basis (see Sect. 3.3), the temporal trends between the two spatial resolutions are in very good agreement, corroborating de Meij et al. (2012). Coarser grid-cells in contrast to the finer spatial resolution meet the data availability threshold (≥ 60 months) (Fig. S4) followed for the calculation of temporal trends because of the more extensive spatiotemporal coverage of MIDAS. MIDAS meets adequately the temporal criteria (Sect. 2.2) both at fine (Fig. S4a) and coarse (Fig. S4b) spatial resolutions, providing grid cells of long-term AOD/DOD time series along with significant AOD (Figs. 1a and 1c) and DOD (Figs. 1b and 1d) tendencies. Trend analysis for the coarse grids yields a superior number of significant AOD tendencies globally (Figs. 2a and 2b). In addition, new and significant declining AOD trends are observed in East Asia, particularly across Southeast Asia, the Yellow Sea, the Sea of Japan, and the North Pacific Ocean. Similarly, AOD trends are reported in the Southern Arabian Sea and the North Atlantic Ocean nearby the coast of Venezuela. Over the Southern Pacific, Atlantic and the Indian Ocean, increasing numbers of negligible AOD trends are calculated.

Voss and Evan (2020) generated two global DOD datasets using MODIS retrievals, combined with reanalysis data and AERONET inversion retrievals. They estimated the decadal DOD trends (see their Figs. 11a and 11b) based on MODIS/Terra (2001-2018) and MODIS/Aqua (2003-2018) data projected at an equal lat-lon 1° spatial resolution. In order to compare the findings in this study against Voss and Evan (2000), only arithmetic DOD trends are used at the same grid-cell spatial resolution (Fig. S1b). In addition, since MIDAS dataset relies on MODIS-Aqua retrievals (Sect. 2.1), only their DOD MODIS/Aqua dataset is used for comparison. Over the Sahara Desert, Bodélé Depression and Thar desert, identical significant trends in terms of magnitude and sign are recorded in both studies. Over Arabian Peninsula, the calculated trends here are common in terms of sign but lower in terms of magnitude. Trend inconsistencies are also revealed because of a) the derivation algorithm of DOD, b) the trend detection methodology, c) the different study periods, and d) the temporal filtering criteria. More specifically, the current study reports declining DOD trends along the Mediterranean Basin, while Voss and Evan (2020) did not find any significant trends. On the other side, they reported strong positive trends over Tropical Atlantic Ocean, sub-Sahel, Northeast Middle East and Northeast Caspian and Aral Sea which is not the case here.

3.1.3 Filtering vs. non-filtering trends

The third sensitivity analysis of this section concerns the calculation of temporal trends using filtered (Fig. 1) and non-filtered (Fig. S5) data at fine spatial resolution. Here, the AOD/DOD trends are calculated by applying two consecutive temporal filters (Sect. 2.2). If a similar procedure for calculating trends without considering any filtering, each grid point provides equal or higher number of available months. For example, months with more than one daily measurement are retained for trend analysis. More specifically, the total data availability on the entire global grid increases from 36% (filtered) to 83% (non-filtered). More particularly, in areas with extended cloud coverage, the number of available months (and years) has been substantially increased.

According to Eq. (3), σ_ω (Figs. S6 and S7) and the statistical significance (Figs. S8 and S9) of the trend is controlled by σ_N, φ (Figs. S10 and S11) and n. Across the desert areas, the number of filtered months (Fig. S4a) is adequately high and very close to the non-filtered case. Thus, no trend differences in magnitude and sign are recorded. Over maritime and continental dust affected areas (non-desert), new statistically significant AOD and DOD trends are represented (Fig. S11). Firstly, the number of significant DOD pixels has been significantly increased (Figs. S11b and S11d) but the majority of the new trends are mainly neutral located over oceanic territories (yellow pixels). New positive DOD tendencies are observed over Tropical Atlantic and India while new negative trends are recorded across Southeast China. Secondly, the significant AOD trends grid points are also strongly increased. New decreasing AOD trends are observed over USA, China and Philippine Sea. In addition, new AOD increasing trends are recorded over Tropical Atlantic, North Pacific (West of Mexico), Arabian Sea and the oceanic area between 30.0ºS and 60.0ºS. The analysis presented above has been also conducted for coarse spatial resolution (Fig. S12), giving similar results. Despite the increase in available monthly data, trend analysis without temporal filtering may lead to erroneous and not representative results either for AOD or DOD. In the following sections, only the filtered geometric-based DOD and AOD trends at fine spatial resolution are shown.

3.2 Seasonal trends

Dust aerosols' burden is subjected to strong intra-annual and interannual variations with different cycles depending on the source or downwind region (Gkikas et al., 2021, in preparation). Here, the seasonal DOD tendencies at a global scale (Fig. 2) are calculated based on the methodology proposed by Hsu et al. (2012). The corresponding seasonal AOD trends are depicted in Fig. S13.

https://doi.org/10.5194/acp-2021-418
Preprint. Discussion started: 28 June 2021

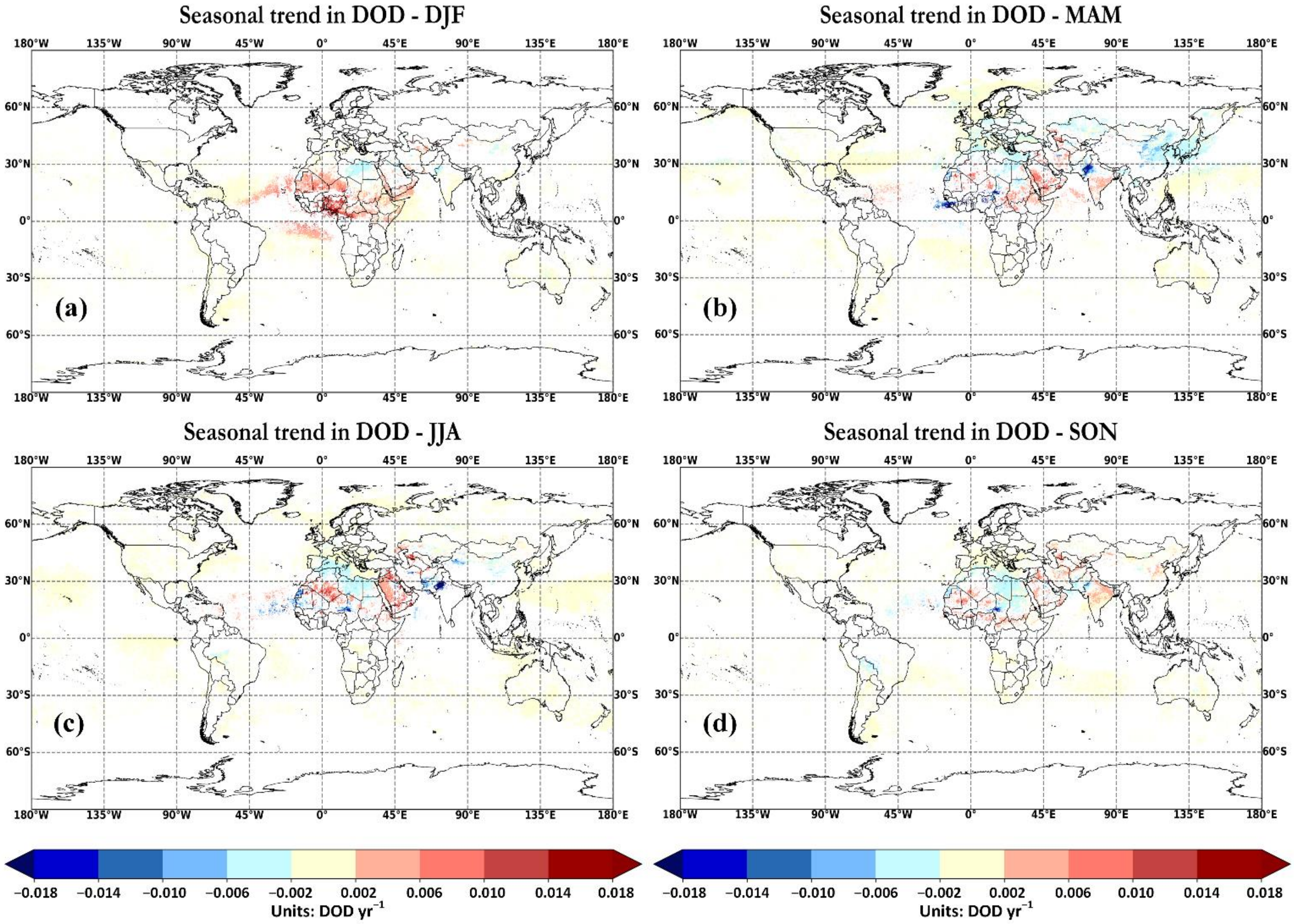

Figure 2: Seasonal geographical distributions of DOD temporal trends at (a) December-January-February (DJF), (b) March-April-May (MAM), (c) June-July-August (JJA) and (d) September-October-November (SON).

The detection of the statistical significance of the calculated trends based on Weatherhead et al. (1998) cannot be applied here due to the 9-month gap among the seasons. Therefore, an alternative approach is followed by calculating the seasonal trends using a simple linear regression model on the DOD anomalies and identifying the statistically significant trends based on the two-sided Student's t-test. The null hypothesis of the t-test assumes a non-significant temporal trend under a defined confidence level (here is 95%). The total number of months for each season is displayed in Fig. S14. Only the grid points with more than 13 available months (13 from 45 total months) are retained. In regions where specific meteorological phenomena exist, such as the summer monsoon in India, the seasonal trends are not calculated due to data gaps, attributed to the extended cloud coverage. The global and seasonal analysis reveals many regions with significant DOD trends (Figs. 1 and 2) which are used to define regional domains (Fig. 3).

https://doi.org/10.5194/acp-2021-418
Preprint. Discussion started: 28 June 2021

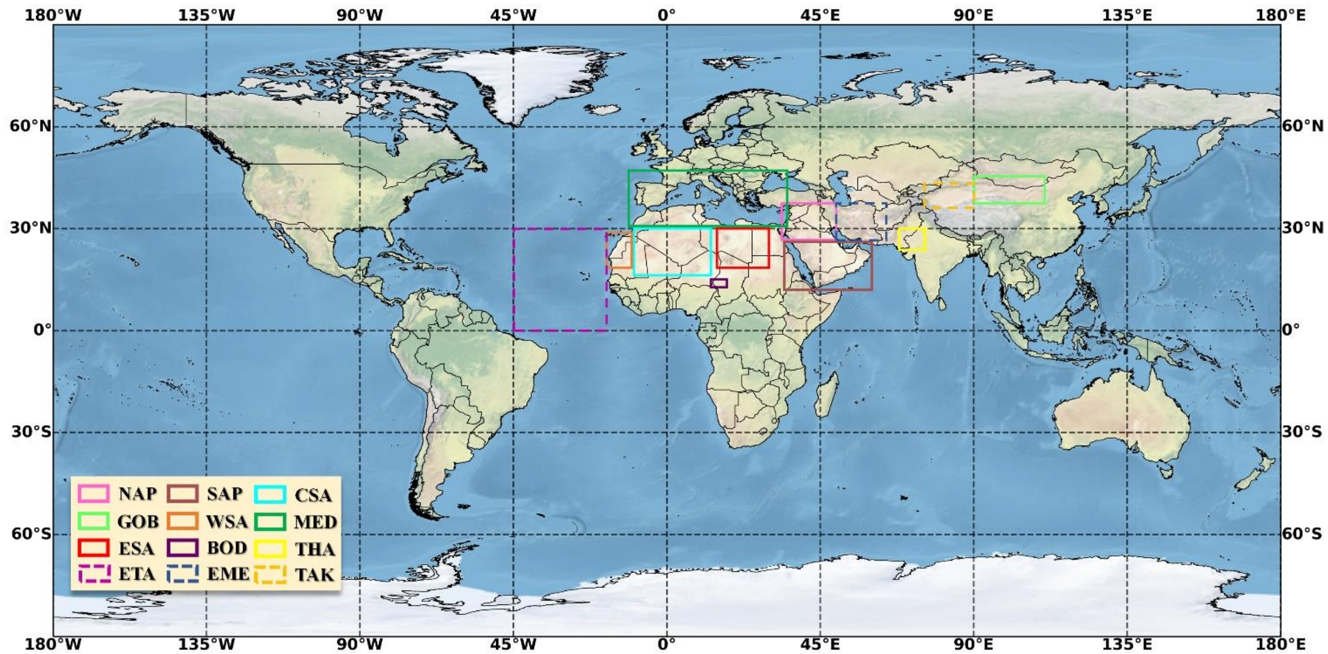

Figure 3: Regions of interest for seasonal and regional analysis: North Arabian Peninsula (NAP), South Arabian Peninsula (SAP), Central Sahara (CSA), Gobi Desert (GOB), West Sahara (WSA), Mediterranean (MED), East Sahara (ESA), Bodélé Depression (BOD), Thar Desert (THA), East Tropical Atlantic (ETA), Eastern Middle East (EME) and Taklamakan Desert (TAK). Solid rectangles indicate the regions are included in regional analysis (Sect. 3.3) while solid and dashed rectangles are for seasonal analysis.

Sahara Desert, the most active aeolian natural dust source of the planet, is of great interest for intra-seasonal DOD variations. In its central sector, increasing trends are recorded throughout the year (maximum positive value in JJA) (Table S1). On the contrary, negative seasonal DOD trends appear in the majority regions across North Africa (Fig. 2). The western and eastern parts of the Sahara Desert present strong declining trends maximized during boreal summer (Table S1). From spring to autumn, in the Bodélé Depression, substantial decreasing trends are recorded (Table S1). Over the period 2001-2012, dust emissions in the broader area of the Bodélé Depression were decreased in summertime, which was attributed to the increased rainfall, caused by the positive trends of the Sahara heat lows (SHL), the warm phase of Atlantic Multi-decadal Oscillation (AMO) and the decreasing trends in terms of occurrence and intensity of nocturnal low-level jets' (NLLJ) (Shi et al., 2021). Surface wind speed also affects dust emissions across North Africa (Evan et al., 2016). Surface wind speed and NLLJ are the principal drivers for the interannual variation of dust emissions across Western Sahara, while in summertime dust emissions decreased during 2001-2012 (Shi et al., 2021). The eastern sector of North African coast (North Libya and Egypt) presents moderate negative trends maximized in winter (down to −0.014 yr^{-1}) and spring (down to −0.011 yr^{-1}). In the western sector of North African coast (north Algeria and Tunisia) strong significant declining trends are observed in summer (down to −0.035 yr^{-1}) (Fig. 2c). The dust sources residing in North African coast are strongly influenced by the surface wind speed, NLLJ, Harmattan surge and the tracks of the Mediterranean depressions (Shi et al., 2021).

https://doi.org/10.5194/acp-2021-418
Preprint. Discussion started: 28 June 2021

According to Gkikas et al., (2021, in preparation), MIDAS climatology detected transatlantic transport of mineral dust particles. Across the Gulf of Guinea and mid-Atlantic, relatively high DODs are documented in boreal winter (Fig. 2a), ranging from 0.1 to 0.2 (up to 0.6). According to Fig. 2a, strong positive DOD trends are shown over Gulf of Guinea (up to 0.047 yr^{-1}). In this season, strong northeasterly winds (Harmattan) transport intense loads of Saharan dust towards Nigeria and the Gulf of Guinea (Washington et al., 2006). However, the trend magnitude along the Gulf of Guinea as well as in the northern regions (from Ghana to Cameroon) seems to be unreliable. The applied MERRA-2 dust fraction in MIDAS overestimates the CALIOP retrievals across this region, providing higher DOD values (Gkikas et al., 2021). In the case of AOD (Fig. S13a), identical positive trends as DOD are shown in winter. The overestimation of DOD across this region leads to substantial high DOD trend and it is related to total aerosols load. Interestingly, substantial negative DOD trends (down to −0.045 yr^{-1}) are recorded during springtime in an area among Guinea, Sierra Leone and North Atlantic Ocean (Fig. 2b), while positive tendencies are documented over Tropical Atlantic Ocean in DJF (Table S1). Over the region extended from North Atlantic Ocean to Eastern Caribbean Sea (Lat: 10.0 ºN−18.0ºN; Lon: 70.0 ºW−45.0 ºW), moderate positive trends are documented predominantly in MAM (up to 0.01 yr^{-1}) and JJA (up to 0.008 yr^{-1}). The statistically significant DOD trends across this area could be explained by the intense dust transport from North African along the Atlantic Ocean reaching Caribbean Sea (Alizadeh-Choobari et al., 2014c; Gläser et al., 2015). Across the aforementioned region, summer DODs are intertwined with tropical Atlantic cyclone activity. More specifically, Caribbean DOD during summer is negatively correlated to Atlantic accumulated cyclone energy and Atlantic Meridional Mode index (Xian et al., 2020).

Middle East areas, extending from South Arabian Peninsula to eastern Iran, tends to be dustier in all seasons (Table S1). South Arabian Peninsula reveals principally positive seasonal trends (Fig. 2). More specifically, the southwestern region of Oman presents the highest increasing trends for all seasons (up to 0.026 yr^{-1}). Similarly, high positive trends in MAM (up to 0.015 yr^{-1}) and JJA (up to 0.018 yr^{-1}) are documented over the western part of Saudi Arabia. Negative tendencies are observed for all seasons in a region located at the north of Oroug Bani M’aradh Wildfire Sanctuary (South Saudi Arabia) including strongly negative DOD trends in summer (down to −0.020 yr^{-1}) and spring (down to −0.019 yr^{-1}). In the northern part of Arabian Peninsula, positive trends are detected predominantly in JJA and SON. Dust activity across Arabian Peninsula is strongly influenced by the intensity of the northwesterly Shamal winds, favored by the low precipitation amounts during summer (Yu et al., 2015). The long drought (Notaro et al., 2015) along with the cool Tropical Indian Ocean and Mediterranean Sea temperatures (Yu et al., 2015), which enhanced Shamal wind, could regulate the summer DOD trends across Arabian Peninsula. During springtime, La Niña events constitute the principal drivers for the dust activity by reducing the rainfall amounts over Rub’ al Khali Desert; one of the most active dust sources across Arabian Peninsula (Yu et al., 2015). Strong positive trends (up to 0.026 yr^{-1}) are encountered in MAM and JJA over Iraq, while significant increasing trends are recorded for all seasons across Eastern Iran, with the most positive values in spring (up to 0.020 yr^{-1}). However, a hotspot of strong declining trends exists in southeastern area of Iran (34.5°N, 54.5°E) with the most negative values in JJA (down to −0.029 yr^{-1}) and SON (down to −0.025 yr^{-1}). Moderate negative DOD trends are documented during the summertime (down to −0.01 yr^{-1}) across the Alboran Sea (western Mediterranean). The dust aerosol burden has also been decreased in the eastern part of

Mediterranean Sea during spring (down to -0.006 yr^{-1}, from Lybia and Egyptian coasts to Aegean Sea) and autumn (down to -0.005 yr^{-1}, across the Gulf of Sidra).

Statistically significant positive DOD trends are detected across the intersection of Kazakhstan, Uzbekistan and Turkmenistan, in the northeastern Caspian Sea shore. At all seasons, the DOD trends exceed 0.011 yr^{-1} while the maximum trends are recorded in summer (up to 0.035 yr^{-1}) and spring (up to 0.019 yr^{-1}). These findings substantiate the positive decadal DOD trends (~0.18 decade^{-1}) of Voss and Evan (2020) and could be attributed to the amount of drawdown (~-6.72 cm yr^{-1}) in the Caspian Sea level during 1996-2015 (Chen et al., 2017). Central, South and East Asia constitute another regions of interest in which robust DOD trends are encountered (Fig. 2). The maximum negative values are depicted over the Thar Desert in JJA and MAM (Table S1). It must be highlighted that the maximum decreasing trends are detected during the high-dust season of Thar Desert (Proeastakis et al., 2018). The reduction of dust load during the pre-monsoon (MAM) could be attributed to the increase of the rainfall and soil moisture levels, acting in favor of wet dust deposition as well as decreasing the dust erosion (Pandey et al., 2017; Jin and Wang, 2018; Lakshmi et al., 2019). Moreover, reductions in dust emissions are recorded during summertime, which are strongly linked to soil moisture and wind speed (Shi et al., 2021). In Northwest China (Central Asia) lies the Taklamakan Desert, where non-significant annual trends are documented (Fig. 1). However, significant seasonally negative DOD trends are observed (Fig. 2) during specific seasons (Table S1), indicating the most descending records predominantly in summertime. Additionally, over the Gobi Desert and East Asia strongly negative DOD tendencies are documented mainly in spring (Fig. 2b), coinciding with their most active dust activity season (Proestakis et al., 2018). The negative DOD trends across Gobi Desert could be attributed to reduced dust emissions, caused by the decrease of surface wind speed which has been recorded between 2010-2016 (Guo et al., 2019).

3.3 Regional trends

The regional DOD and AOD trends are calculated for 9 specific regions of interest (Table 1 and Fig. 3 solid rectangles) as well as globally (GLB), over land (GLB-L) and ocean (GLB-O) (Sect. 3.3.1). The full names of each region as well as the calculated regional DOD trends and their uncertainties are included in Table 1. The comparisons among the geometric vs. arithmetic aggregation method and coarse vs. fine spatial resolution are also investigated for DOD (Fig. 4) and AOD (Fig. S15) regional trends. Since the statistical significance of the trends is strongly influenced by the number of years and the study period, the regional DOD trends are also computed for different time periods considering the systematic change of time period (number of years) and initial year (Fig. 5).

https://doi.org/10.5194/acp-2021-418
Preprint. Discussion started: 28 June 2021

Atmospheric Chemistry and Physics
Discussions

Table 1: Global and regional temporal DOD trends based on MIDAS dataset. The trends with the ratio $|\omega/\sigma_{\omega}|$ higher than 2.0 are statistically significance at 95% confidence level. The star symbol corresponds to statistically significant regions under the 95% confidence level. The domains of the regions are represented in Fig 3.

Region	Acronym	Trend (ω, DOD yr^{-1}) × 10^{-3}	Uncertainty (σ_{ω}) × 10^{-3}	$\lvert\omega/\sigma_{\omega}\rvert$
Global land & ocean	**GLB**	0.022	0.12	0.19
Global land	**GLB-L**	0.082	0.25	0.33
Global ocean	**GLB-O**	−0.017	0.069	0.24
North Arabian Peninsula	**NAP**	0.60	1.3	0.45
South Arabian Peninsula	**SAP**	1.80	1.2	1.5
Central Sahara	**CSA**	2.1	0.87	2.4*
Gobi Desert	**GOB**	−0.71	0.39	1.8
West Sahara	**WSA**	−0.95	0.85	1.1
Mediterranean	**MED**	−1.1	0.30	3.8*
East Sahara	**ESA**	−1.8	0.61	3.0*
Bodélé Depression	**BOD**	−5.5	2.6	2.1*
Thar Desert	**THA**	−5.3	1.9	2.8*

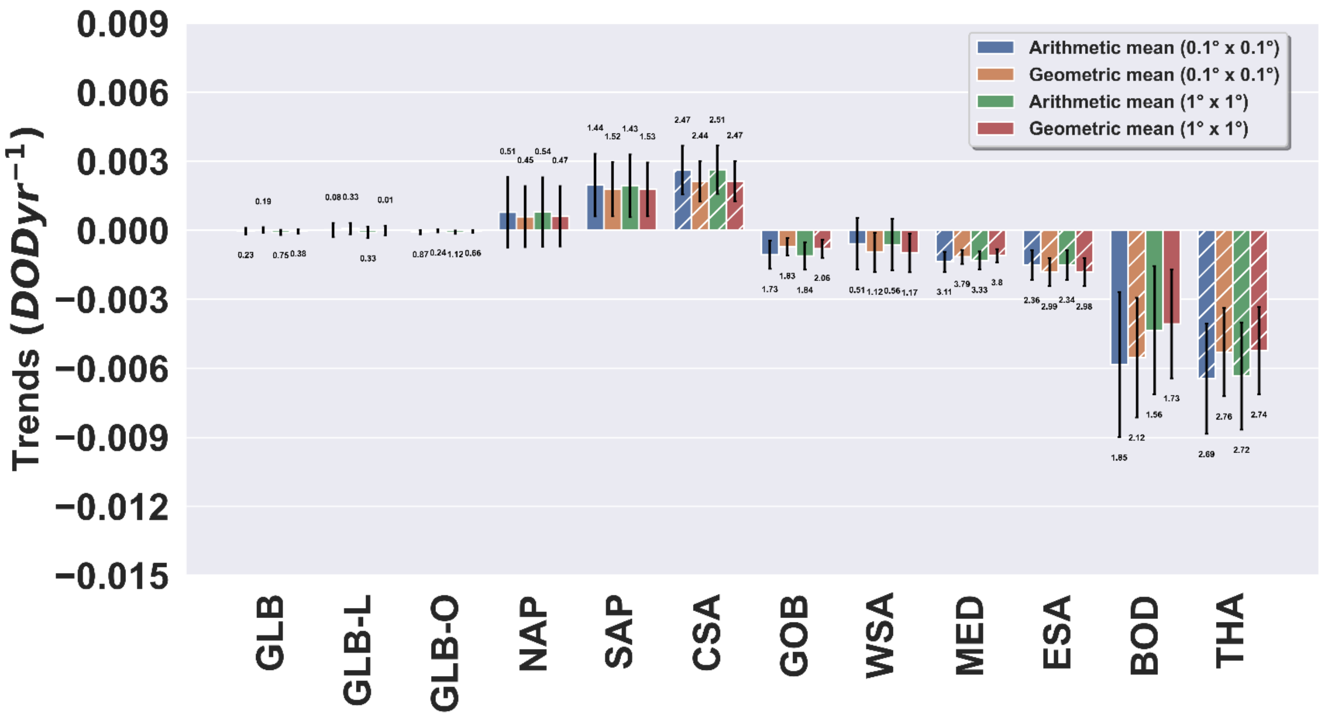

Figure 4: Bar-plots indicating the DOD regional temporal trends. The hatched bars represent regions with significant DOD trends ($|\omega/\sigma_{\omega}| > 2.0$). The error bars denote the uncertainty of DOD trends based on Eq. (3) (Sect. 2.2).

The explanation of the temporal evolution of calculated trends shown in Fig. 5 is presented in the next section for individual regions.

https://doi.org/10.5194/acp-2021-418
Preprint. Discussion started: 28 June 2021

Atmospheric Chemistry and Physics Discussions

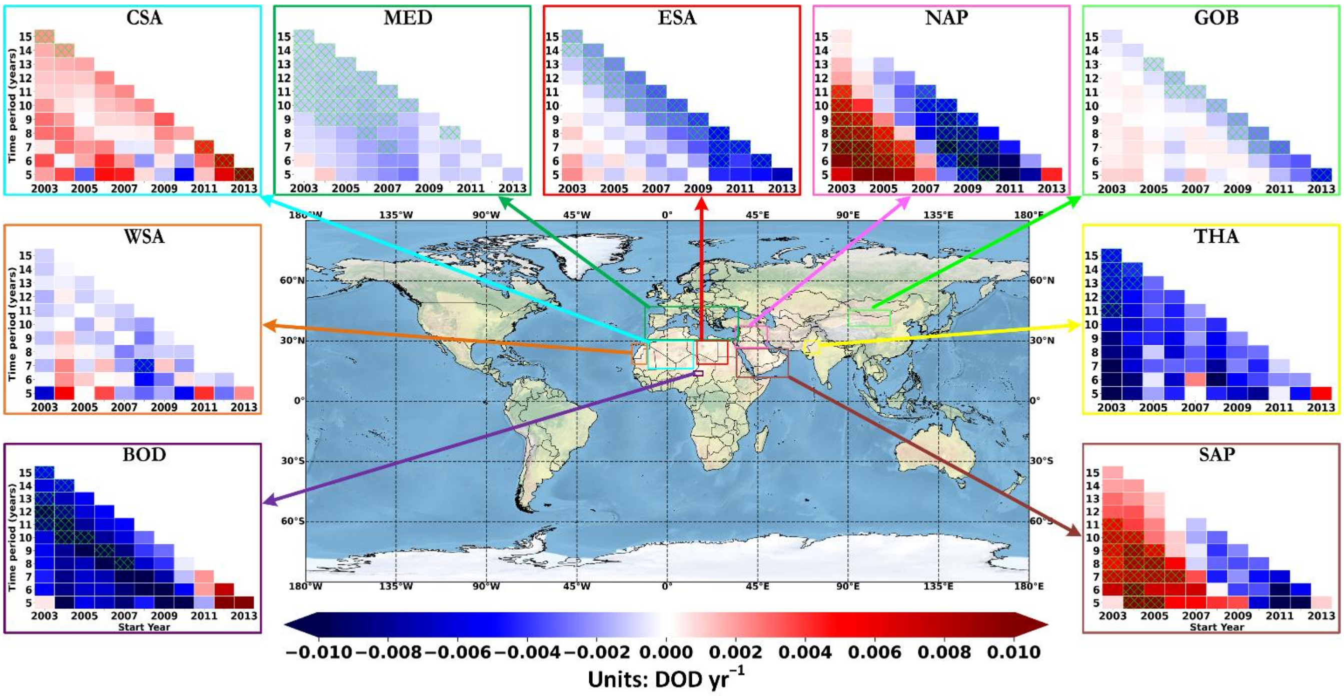

Figure 5: Regional DOD trends at different time intervals, with at least 5-year time series. The acronyms full names are documented in Table 1. YY' axis shows the number of trends included in the analysis, while XX' the starting year.

3.3.1 Global land and ocean

Small global DOD trends are recorded during the study period both over land and ocean (Table 1). However, distinguishable DOD trends are detected at specific regions. Prior studies have focused on satellite-based measurements detecting statistically significant AOD trends at global scale. In this study, significant AOD trends are revealed over GLB-O and GLB (Fig. S15). Over oceanic areas, AOD trends based on MODIS Collection 6.0 are reported to be equal to 0.0050 decade^{-1} and 0.0020 decade^{-1} during 2000-2009 and 2000-2015, respectively (Alfaro-Contreras et al., 2017). SeaWiFS AOD retrievals recorded higher annual positive significant trends over ocean (0.00080 yr^{-1}) for a 13-year period (1998-2010) (Hsu et al., 2012). Recently, significant positive tendencies are documented for GLB (0.00066 yr^{-1}) using L3 Collection 6.1 MODIS/Terra measurements spanning from 2001 and 2016 (Che et al., 2019). The differences in trends magnitude among the studies are attributed to the different datasets, aggregation methods and temporal availability.

3.3.2 North Africa

Across North Africa, four sectors have been defined based on the sign of DOD trends. The first one consists of Central Sahara (CSA) where increasing DOD trends are mainly recorded (up to 0.023 yr^{-1}) (Fig. 6c). Voss and Evan (2020) also recorded similar DOD trends, in terms of sign and magnitude, based on MODIS/Aqua dataset over the period 2003-2018. At regional scale, positive significant DOD trends of 0.0021 yr^{-1} determining those of AOD as expected (regional DOD to AOD

https://doi.org/10.5194/acp-2021-418
Preprint. Discussion started: 28 June 2021

Atmospheric Chemistry and Physics Discussions

trend ratio=0.84) due to the predominance of mineral particles in the area among other aerosol species (Fig. 6d). During different time frames, the sign of DOD trends remains mainly positive (Fig. 5), with intense (from 0.0044 to 0.0095 yr^{-1}) and significant results within the 2011- onward periods.

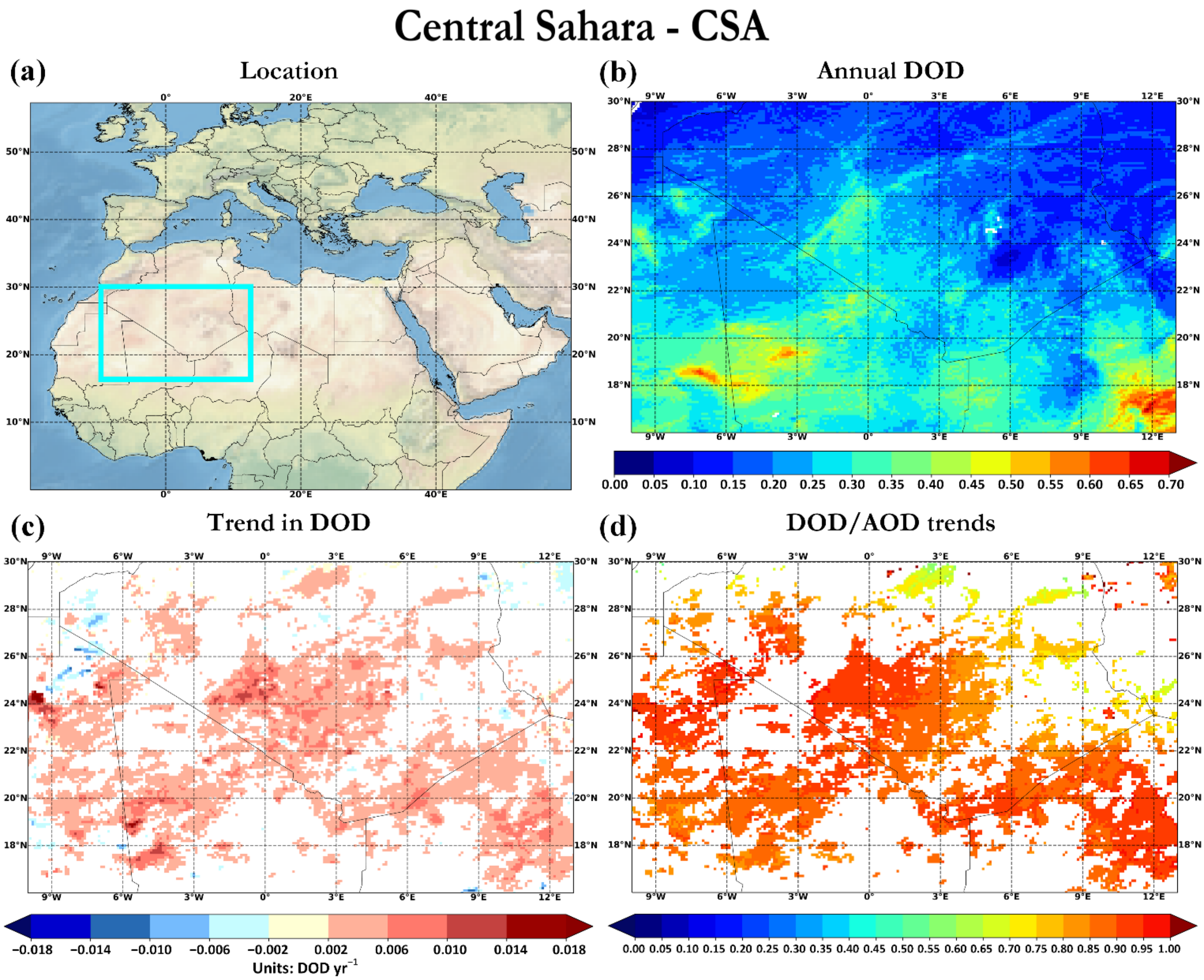

Figure 6: (a) geographical boundaries, (b) annual DOD, (c) DOD geometric trends and (d) DOD to AOD trends ratio, for the Central Sahara.

In westernmost section of the Sahara Desert (WSA), in the majority of grid-cells (~73%) decreasing DOD tendencies are recorded (down to −0.015 yr^{-1}) whereas positive trends (up to 0.009 yr^{-1}) are evident at scattered pixels (~27%) within the domain (Fig. 7c). Overall, the total load (Fig. S15) as well as the dust burden (Fig. 4) have been decreased during the study period, but the magnitude of this reduction is relatively low and not statistically significant. This behavior is consistent

https://doi.org/10.5194/acp-2021-418
Preprint. Discussion started: 28 June 2021

Atmospheric Chemistry and Physics Discussions

regardless the spatial resolution or the approach for the calculation of regional values (i.e., arithmetic or geometric mean) (Figs. 4 and S15). The same DOD trend pattern is also reflected using different time periods (Fig. 5).

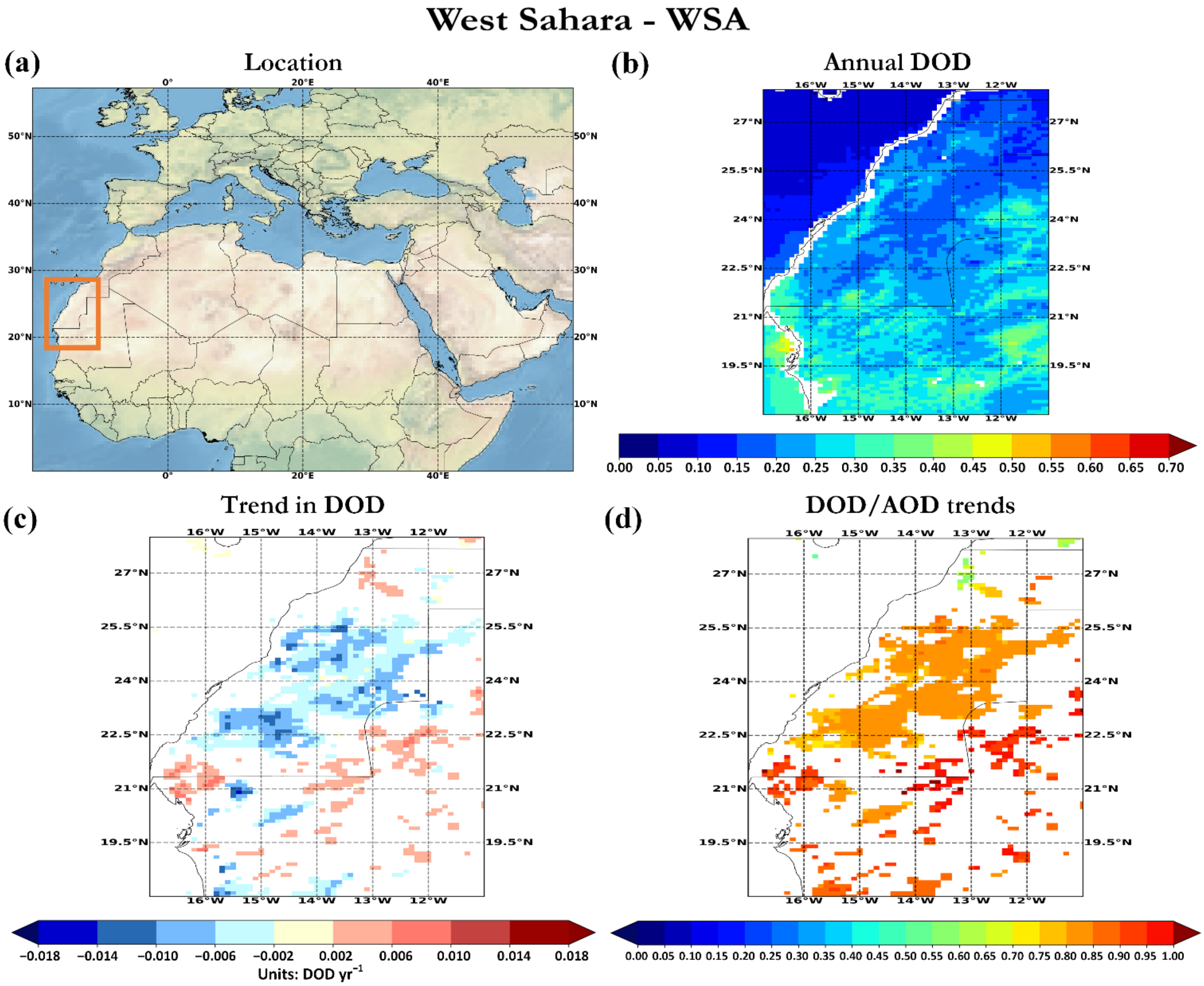

Figure 7: Same as Fig. 6, but for the Western Sahara.

The eastern sector of the Sahara Desert (ESA) records strong negative DOD trends (down to −0.023 yr^{-1}) (Fig. 8c). DOD (Fig. 4) and AOD (Fig. S15) values are revealed identical and significant across this region. Reduction of dust burden has also been recorded from MODIS/Terra dataset according to Voss and Evan (2020). Dust particles affect potentially total AOD across ESA indicating a regional DOD to AOD trend ratio of 1.06. Over the dust-affected areas of the planet, the DOD to AOD trends ratio range from negative (different trend sign) to higher than unity values. Since the dust burden modulate the total AOD over ‘dusty’ regions, the ratio between DOD and AOD is expected around unity. Higher ratios than unity are expected as the non-dust AOD signal decreases or increases and the DOD signal shows a reciprocal pattern. According to Fig.

https://doi.org/10.5194/acp-2021-418
Preprint. Discussion started: 28 June 2021

5, two significant outcomes can be extracted in ESA. The magnitude of significant DOD trends increases (down to −0.0054 yr^{-1}, period: 2012-2017) and the number of necessary years for trend detection decreases with increasing starting years.

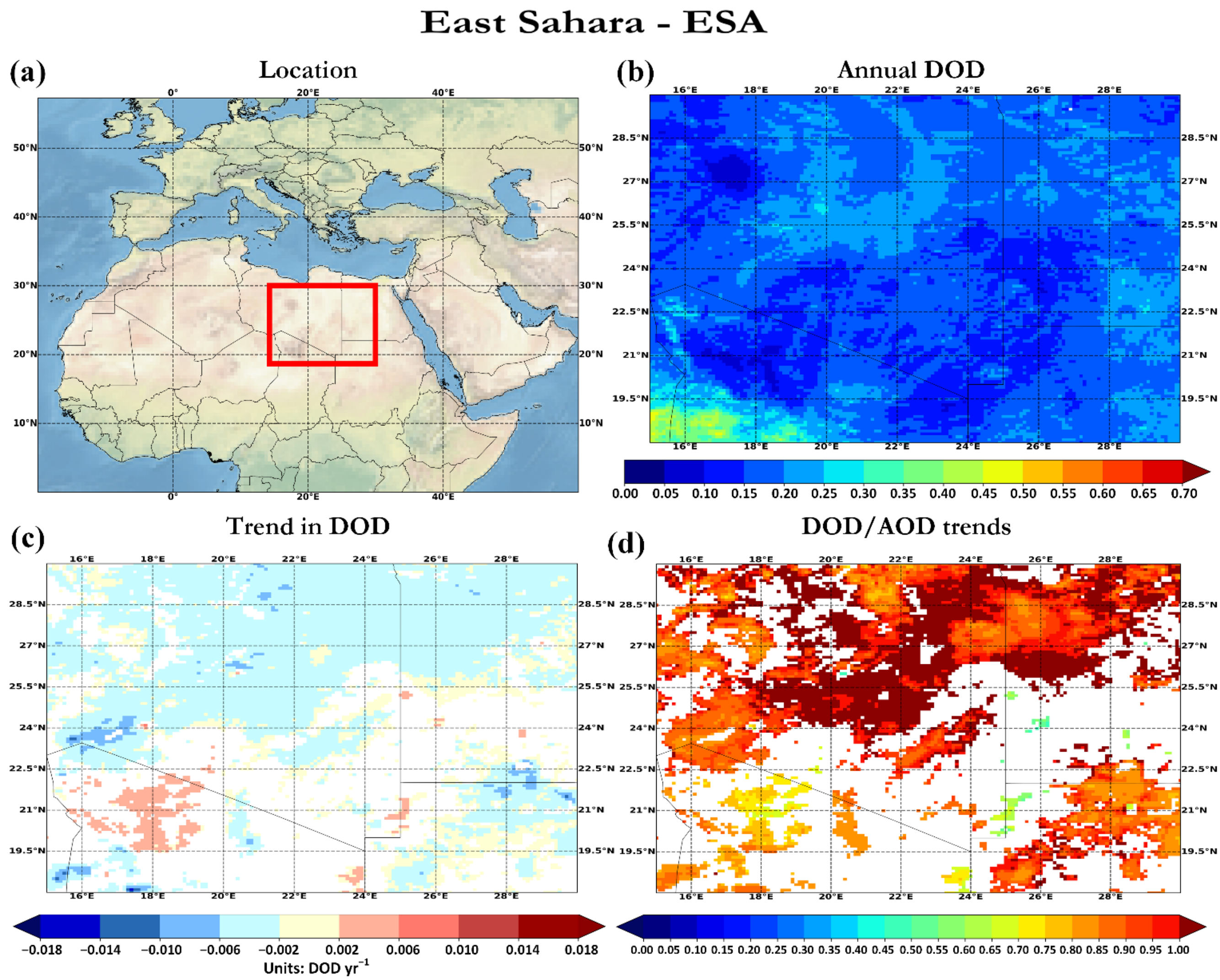

Figure 8: Same as Fig. 6, but for the Eastern Sahara.

Within the study period, the regional dust load decreases (−0.0055 yr^{-1}) in the Bodélé Depression (BOD) consisting the most active aeolian dust source of the planet (Prospero et al., 2002; Washington et al., 2006; Todd et al., 2007; Gkikas et al., 2021, in preparation). DOD trends range from −0.021 yr^{-1} to −0.003 yr^{-1} (Fig. 9c), corroborating the findings of the Voss and Evan (2020). For starting years between 2003-2010 the dust aerosol burden decreased (Fig. 5), with the most negative trend during 2007-2014 (−0.015 yr^{-1}). As the starting year increases and the length of time intervals decreases, the magnitude of DOD trends become weaker. More specifically, the sign of DOD trends is shifted using 2011-2013 as starting years, but the results are not statistically significant. The latter indicates that DOD over the most active dust source of the planet becomes more intense over the last years. Prior studies concluded that changes in total aerosol loading over Sahara Desert are not determined from the changes in aerosol emissions but are regulated from meteorological parameters such as precipitation (Pozzer et al., 2015) and wind speed (Che et al., 2019). More specifically, the increase of precipitation amount, and the decrease of wind speed levels reduce the dust emissions. During the high dust seasons, the interannual variation of dust emissions is affected by wind speed and the NLLJ (in the southern Sahara dust sources) as well as by the Harmattan surge and Mediterranean depressions (in the northern Sahara dust sources) (Shi et al., 2021).

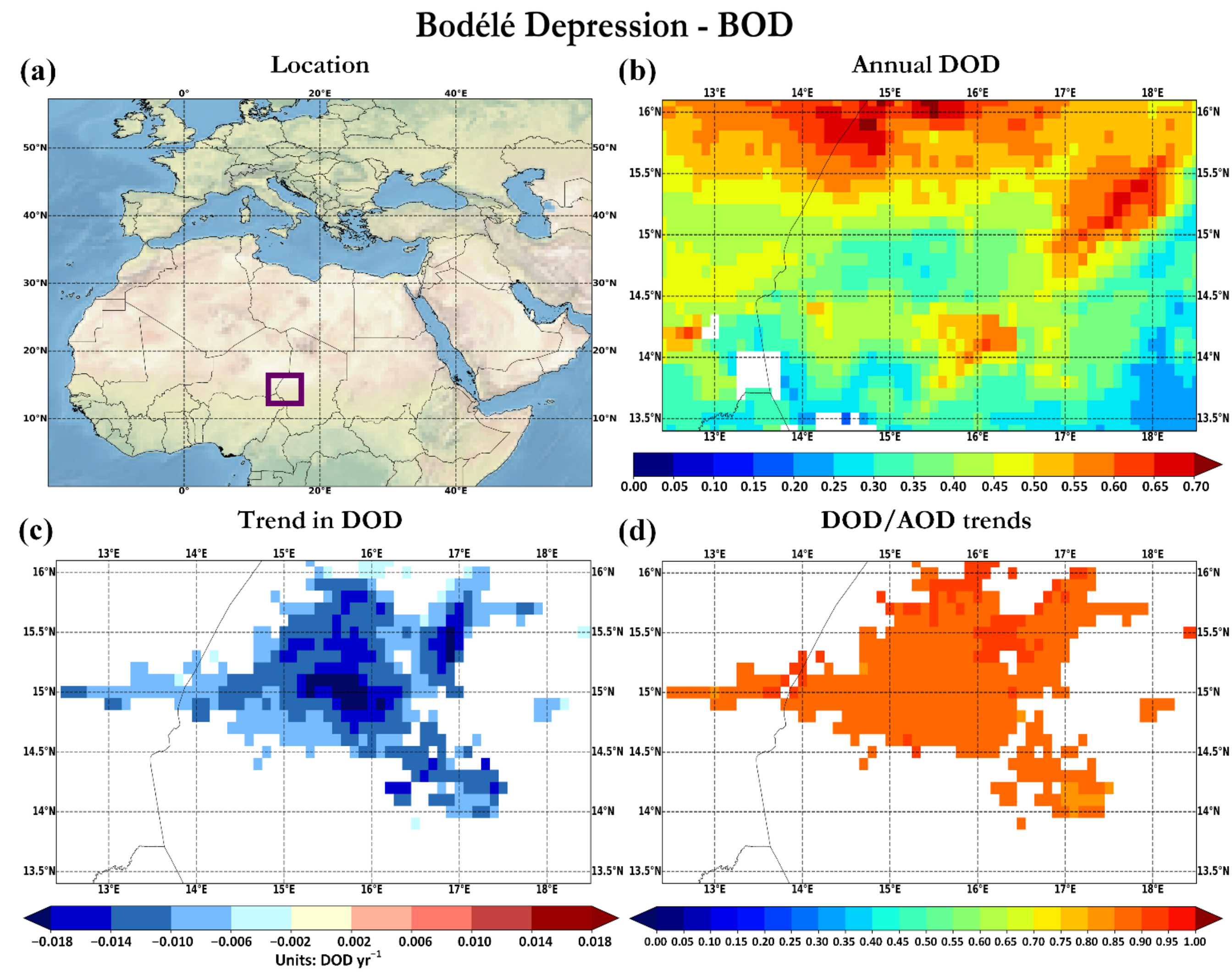

Figure 9: Same as Fig. 6, but for the Bodélé Depression.

https://doi.org/10.5194/acp-2021-418
Preprint. Discussion started: 28 June 2021

Atmospheric Chemistry and Physics
Discussions

3.3.3 Arabian Peninsula

The regional DOD tendencies over the Arabian Peninsula are presented separately for the northern (NAP) and the southern (SAP; including Jordan, Iraq and Syria) sectors. In both regions, positive trends (non-significant, Fig. 4) are computed which are stronger in the southern parts of the Arabian Peninsula.

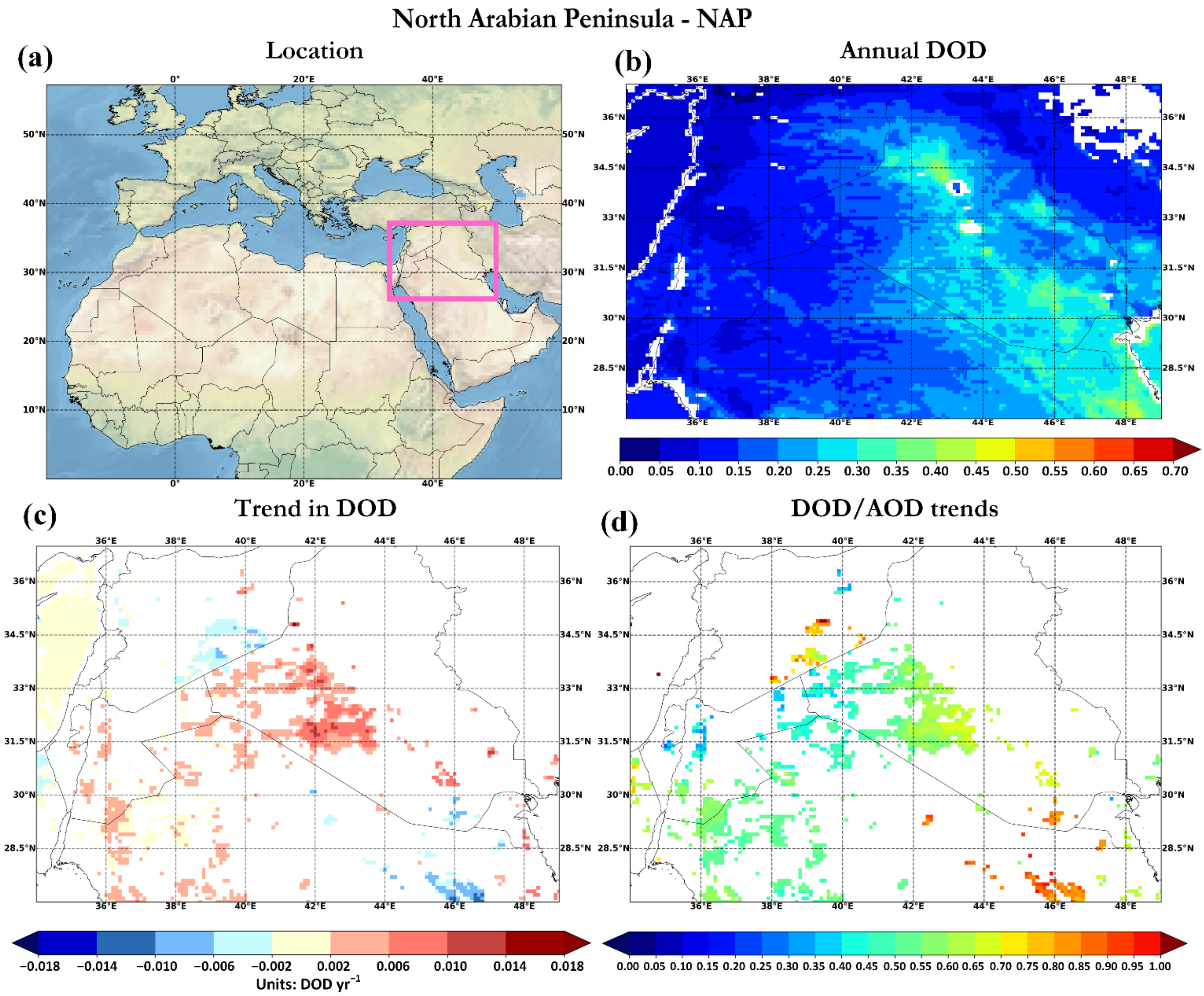

Figure 10: Same as Fig. 6, but for the North Arabian Peninsula.

Across this region, the dust burden (Fig. 4) has been increased during the study period (2003 – 2017). The systematic variation of the year period revealed that dust burden follows a positive significant trend for years up to 2013 (Fig. 5). Afterwards, the reduced aerosols burden indicating strong negative DOD trends for time periods starting around 2009 and finishing in 2017 (Fig. 5). These findings do not contradict with the revealed regime shift in Arabian dust activity discussed in

https://doi.org/10.5194/acp-2021-418
Preprint. Discussion started: 28 June 2021

Atmospheric Chemistry and Physics Discussions

Notaro et al. (2015). The increased dust activity is also reflected to MIDAS DODs between 2008 and 2012, recording increased and stable annual DOD values (~0.2). Onwards, the dust burden has been decreased resulting to negative DOD tendencies. The regional calculations showed non-significant positive regional DOD trends. However, within the study period, the regional AOD trends are positive and statistically significant for all approaches (Fig. S15). Klingmüller et al. (2016) documented that the increasing AOD trend are displayed during 2001-2012 period whereas onwards AOD values follow a decreasing tendency. The regional analysis of DOD trends in this study coincides with their findings (Fig. 5). Frequently existing dust particles across Arabian Peninsula are strongly affect the AOD trends, recording moderately high DOD to AOD trend ratios around 0.65 (Figs. 10d and 11d). These ratios are lower than those of North Africa (Sect. 3.3.2) due to the presence of non-dust aerosol species. Both increases in DOD and non-dust AOD explain the moderate in magnitude trend ratios.

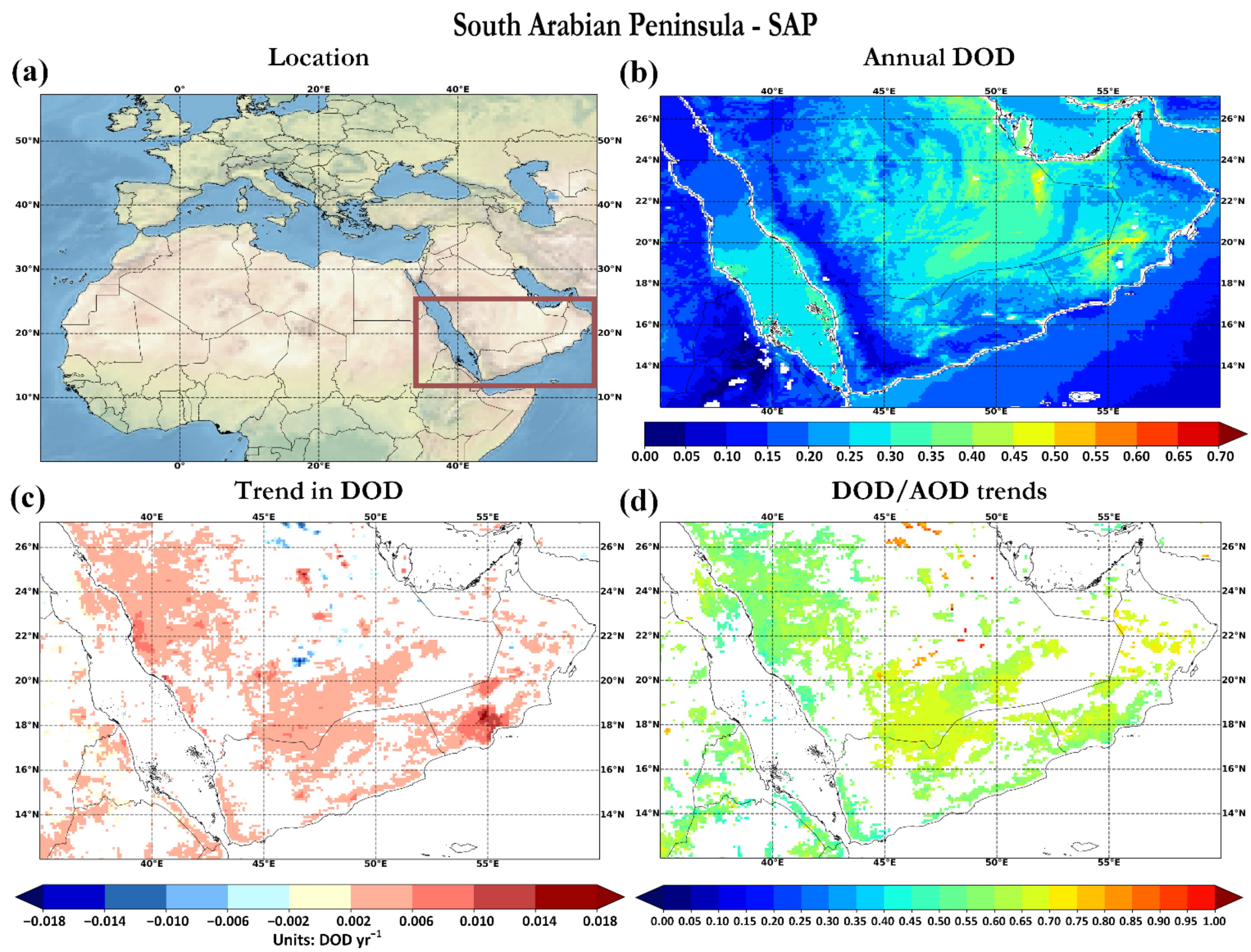

Figure 11: Same as Fig. 6, but for the South Arabian Peninsula.

https://doi.org/10.5194/acp-2021-418
Preprint. Discussion started: 28 June 2021

In the last few decades, compelling inter-annual dust activity is documented in the Arabian Peninsula (Notaro et al., 2015). Numerous studies examined the temporal variability of aerosol loads in the Middle East, showing strong ascending tendencies (de Meij et al., 2012; Hsu et al., 2012; Yoon et al., 2014; Pozzer et al., 2015; Klingmüller et al., 2016; Che et al., 2019; Wei et al., 2019). Klingmüller et al. (2016) revealed that the positive AOD trends in Middle East are linked to decreasing trends of Ångström exponent (AE) and fine mode fraction (FMF). The AE and FMF decreasing tendencies indicate the impact of coarser particles, such as mineral dust, on AOD increasing trend in Saudi Arabia, Iraq and Iran. These findings are further verified by the increasing DOD trends documented in this study during the same study period (Fig. 5). Moreover, Klingmüller et al. (2016) implemented a multivariate linear model for annual AOD in order to identify the linkage of AOD trends with critical parameters such as the precipitation, the surface soil moisture and the surface wind speed. Soil moisture is the major controlling parameter in Saudi Arabia and Iraq whereas precipitation dominates in Iran. For all regions, the addition of surface wind speed as independent parameter increased the model performance. Moreover, Che et al. (2019) also used a multiple linear regression model to investigate the relationship of AOD with specific meteorological parameters. The most appropriate ones, in terms of statistical significance, are chosen to enhance the model performance. Across Middle East, the major controlling meteorological parameter for AOD variance is the sea level pressure (60.9% of total AOD explained variation) and the wind speed, highlighting the great impact of synoptic systems on dust burden over the area.

3.3.4 Mediterranean

The Mediterranean (MED) basin is a region of great concern due to high inter-annual variability of aerosol loadings and types (Floutsi et al., 2016). In this study, MED presents significant DOD trends ranging from -0.009 yr^{-1} to 0.006 yr^{-1} (Fig. 12c). The regional analysis documents strong declining significant DOD (Fig. 4) and AOD (Fig. S15) tendencies across the MED basin. Negative DOD trends are also revealed during different time periods (Fig. 5). The DOD to AOD trend ratio shows a latitudinal reduction moving from northern African coasts to the northern parts of the Mediterranean (Fig. 12d). Higher ratio values are documented in South Mediterranean-North African coast region (0.3-1.94, median = 0.71) (Lat: 30.0−38.0 °N; Lon: 6.0 °W−30.0 °E) compared to North Mediterranean (0.21-0.91, median = 0.45) (Lat: 38.0−45.0 °N; Lon: 1.0 °W−27.0 °E). Dust particles originated from North African and Middle East deserts driven by low pressure systems (cyclones) can be transported towards MED (Gkikas et al., 2015), providing relatively high AOD values at the southern parts. Mineral particles are recorded mainly in summer, spring and winter in Western, Central and East MED, respectively (Floutsi et al., 2016; Gkikas et al., 2021, in preparation). Across the north sector of MED, lower AOD values are associated to higher FMF values due to the prevailing anthropogenic fine aerosols (Floutsi et al., 2016). The latter could also be observed from the negligible DOD trends there (Fig. 12c).

https://doi.org/10.5194/acp-2021-418
Preprint. Discussion started: 28 June 2021

Atmospheric Chemistry and Physics
Open Access
Discussions

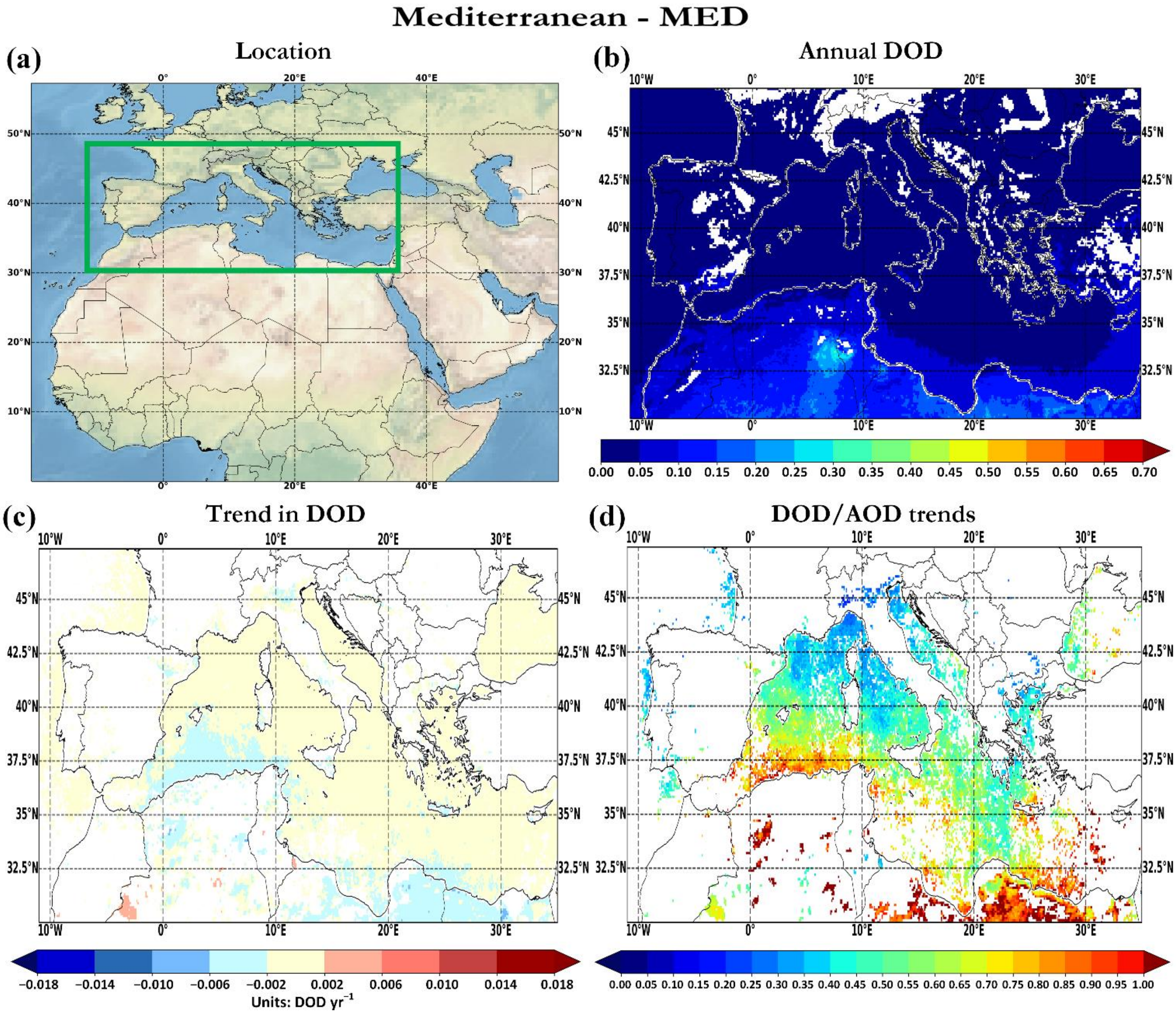

Figure 12: Same as Fig. 6, but for the Mediterranean Basin.

Earlier studies investigated the temporal AOD variability in broader MED basin, reporting declining tendencies for the last two decades (Papadimas et al., 2008; de Meij et al., 2012; Hsu et al., 2012; Yoon et al., 2014; Pozzer et al., 2015; Floutsi et al., 2016; Che et al., 2019). Across this region, Floutsi et al. (2016) reported significant decreasing trends of −0.0030 yr^{-1} over the period 2002-2014. Additionally, Nabat et al, 2013, reported decreasing DOD trends (−0.0045 yr^{-1}) across northern Africa. Both studies corroborate with the findings of this study where the overwhelming majority DOD trends are primarily slightly negative (Fig. 12c).

https://doi.org/10.5194/acp-2021-418
Preprint. Discussion started: 28 June 2021

3.3.5 Thar and Gobi Deserts

Across the west part of Indo-Gangetic Plain, in the northwest area of the Indian Subcontinent, the Thar Desert (THA) is situated. THA region depicts significant DOD trends (down to $-0.017\ yr^{-1}$) (Fig. 13c). According to Fig. 13d, the decreasing AOD trends are strongly modulated by the reduction of dust burden, revealing a moderately high median DOD to AOD trends ratio (0.67). The statistical significance of DOD trends is strongly affected by the variation of the starting year as well as the length of the time interval in which the tendencies are computed (Fig. 5). More specifically, negative and not statistically significant DOD trends are observed for all time periods beginning from 2005. During the last two decades, strong negative temporal trends are recorded for OMI ultraviolet aerosol index (Hammer et al., 2018) along with AOD (Che et al., 2019) and DOD (Voss and Evan, 2020) across THA. The reduction of dust abundance over THA is mainly attributed to the increase of the rainfall and soil moisture enhancing wet dust deposition and reducing dust erosion during pre-monsoon (Pandey et al., 2017; Jin and Wang, 2018).

https://doi.org/10.5194/acp-2021-418
Preprint. Discussion started: 28 June 2021

Atmospheric Chemistry and Physics
Open Access
EGU
Discussions

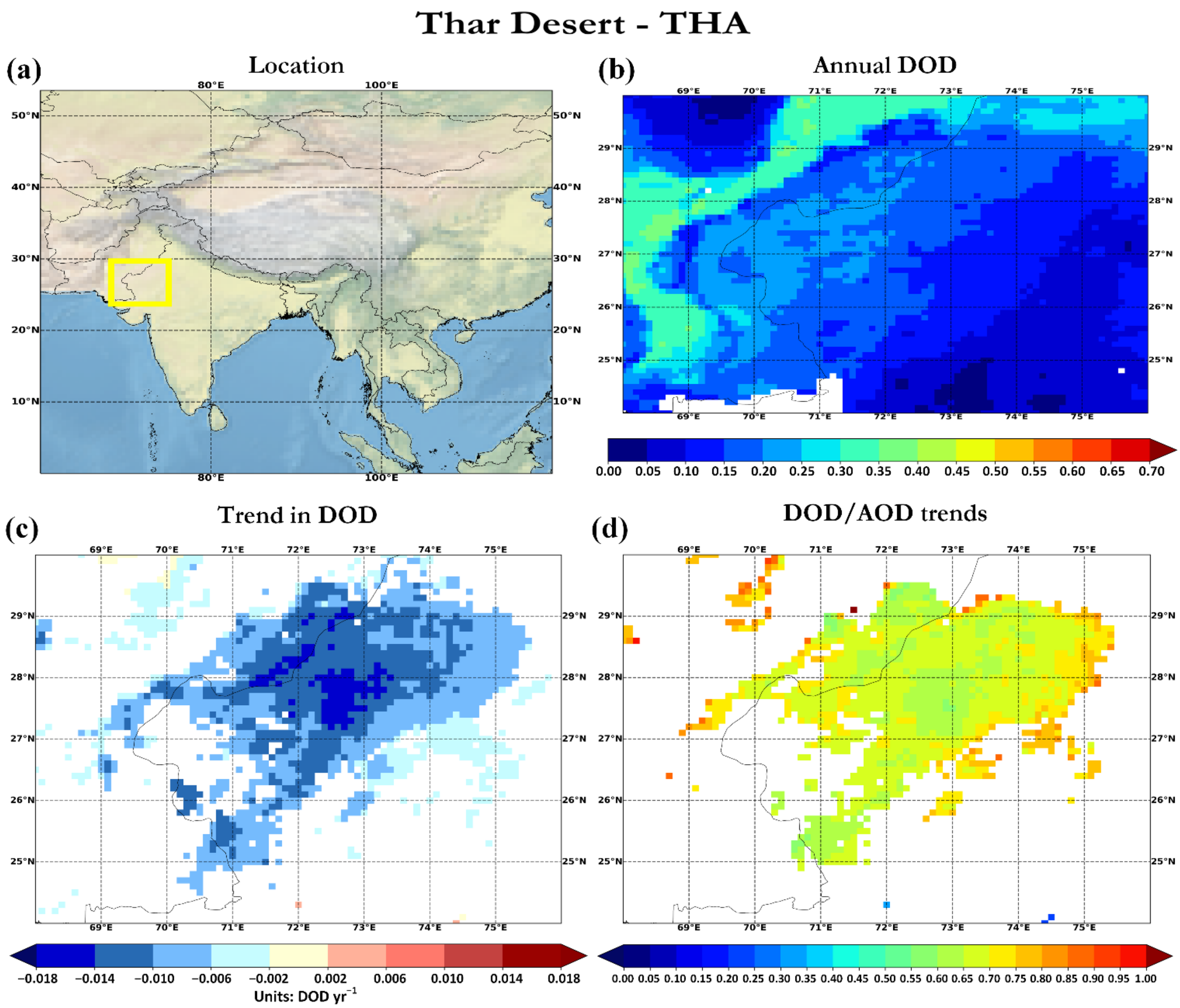

Figure 13: Same as Fig. 6, but for the Thar Desert.

Gobi Desert (GOB) resides between the north part of China and the southern sector of Mongolia (East Asia). In this region, significant DOD trends are reported ranging from −0.011 yr^{-1} to 0.004 yr^{-1} (Fig. 14c). Prior studies have also observed similar AOD (Che et al., 2019) and DOD (Voss and Evan, 2020) trends. The regional analysis showed slightly negative DOD (−0.00071 yr^{-1}) and AOD (−0.0010 yr^{-1}) trends, statistical significance at 90% confidence level ($|\omega/\sigma_\omega|>1.65$, Hsu et al., 2012). However, for years onwards to 2005, significant DOD trends are shown (Fig. 5) across GOB. These temporal DOD trends corroborate with Filonchyk et al. (2019) findings, in terms of trends magnitude. Their regional AOD trends were equal to −0.004 decade^{-1} and −0.002 decade^{-1} for MODIS/Terra and MISR measurements, respectively, during 2000-2017. In addition,

https://doi.org/10.5194/acp-2021-418
Preprint. Discussion started: 28 June 2021

Atmospheric Chemistry and Physics
Discussions

GOB AOD trends are strongly influenced by the presence of dust particles, recording moderate median DOD to AOD trend ratio value of 0.62 (Fig. 14d).

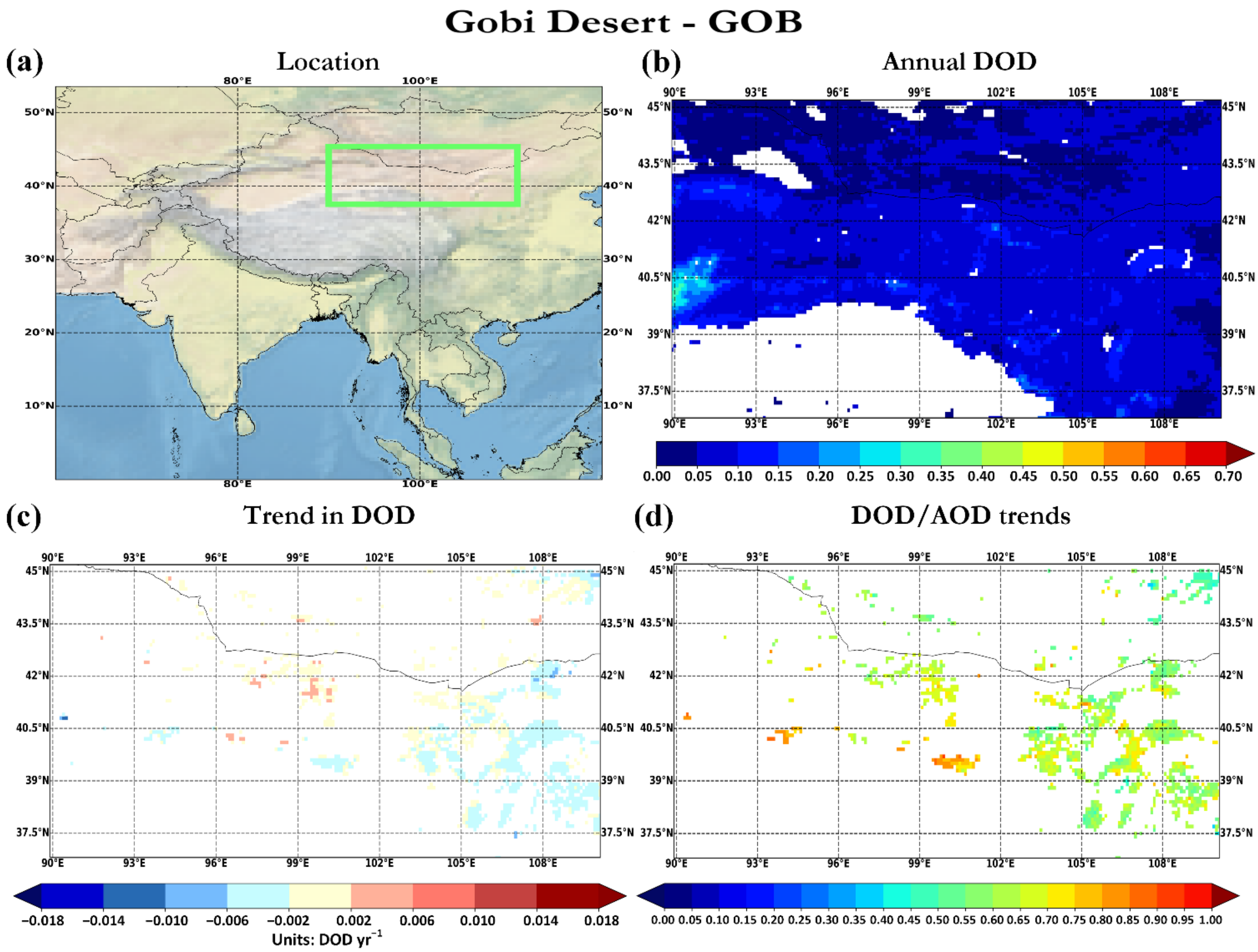

Figure 14 Same as Fig. 6, but for the Gobi Desert.

An et al. (2018) conducted a comprehensive analysis which aimed to investigate the potential factors driving the reduction of sand and dust storms in East Asia between 2006 and 2017. DOD over GOB is strongly related to dust outbreaks with 80% occurred during springtime. In their study, the GOB region included within their region 2 and 3 where the mean surface dust concentration was declined by −29.34 μg m^{-3} yr^{-1} (−14.59 %) and −31.71 μg m^{-3} yr^{-1} (−12.24 %). These declining trends can be related to changes in surface conditions (e.g. vegetation coverage) which are strongly linked to precipitation, soil moisture, ambient temperature and human activities. The increasing trends in vegetation coverage are observed using the Normalized Difference Vegetation Index (NDVI) (region 2 and 3: 0.0006 yr^{-1}) from MODIS retrievals and are strongly related to the ascending tendencies of the precipitation (region 2: 0.005 mm day^{-1} yr^{-1}, region 3: 0.002 mm day^{-1} yr^{-1}) and volumetric soil

https://doi.org/10.5194/acp-2021-418
Preprint. Discussion started: 28 June 2021

moisture at 0-0.1 m depth (region 2: 0.460 yr^{-1}, region 3: 0.316 yr^{-1}). The later positive trends, producing favorable surface conditions and leading to the increase of vegetation coverage and thus may possibly reflects the reduction of surface dust emissions. Another factor that potentially increases vegetation coverage is the increasing surface temperature. Moreover, prevailing synoptic circulation is strongly related to the decrease of frequency and intensity for dust outbreaks over the East Asia during springtime (An et al., 2018). The latter can be associated with the declining of Polar Vortex intensity, north-to-south mean surface level pressure gradient and meridional wind component magnitude. These directly affect the frequency and intensity of dust outbreaks by reducing dust lift and transport.

4 Summary and conclusions

Airborne desert dust particles affect the global and regional climate via their direct and indirect interactions with the incoming solar and outgoing terrestrial radiation. Therefore, the investigation of DOD temporal variations is crucial to assess the climatic role of desert dust. The present study deals with the calculation of the annual and seasonal trends of AOD and DOD, both at global and regional scales over the period 2003 – 2017, relying on the MIDAS fine resolution dataset. Taking advantage of the MIDAS strong capabilities, the DOD trends have been analyzed: (i) at fine and coarse spatial resolutions, (ii) by considering different aggregation approaches (i.e. arithmetic and geometric means), (iii) at annual, seasonal and sub-period time scales (i.e. sliding window) and (iv) along with the contribution to the corresponding tendencies of the total aerosol optical depth. Based on this holistic approach, it is provided a complete overview about the temporal variability of dust loads addressing jointly all the factors determining the sign, the magnitude and the statistical significance of the calculated trends.

Pronounced increasing DOD trends were obtained across the Central Sahara and the Arabian Peninsula whereas opposite tendencies were recorded over the Eastern and Western Sahara, the Thar and Gobi Deserts, in the Bodélé Depression and in south Mediterranean. The sensitivity analysis between coarse and fine spatial resolution resulted lower in magnitude annual AOD/DOD trends at coarse spatial resolution. On a regional basis the AOD/DOD trends represent a very good agreement for both spatial scales. In general, coarse resolution provides better statistics due to cloud presence at 0.1° by 0.1°degrees related pixels, however crucial spatial detail especially close to dust sources is described much better with the fine resolution data analysis. In addition, the use of arithmetic instead geometric mean in trends calculations showed that arithmetic-based trends tend to overestimate the geometric-based trends (from 52.87 to 91.77%). Which is in line with the lower geometric means of DOD compared with the arithmetic ones. The only exception was occurred for AOD at coarse spatial resolution over ocean in which arithmetic-based AOD trends tends to underestimate the geometric-based trends (71.63%).

The seasonal analysis displayed the most positive DOD trends in Central Sahara and Middle East area in summertime. During spring, the strongest reductions of dust burden have been revealed at the Bodélé Depression whereas reverse tendencies have been recorded in the Western and Eastern Sahara and in the Thar and Taklamakan Deserts during summer. Similarly, the most negative trends were observed at spring over the Gobi Desert. Positive trends across the area extending from North Atlantic Ocean to the eastern Caribbean Sea are observed in spring.

Small and non-significant DOD trends were recorded over ocean, land and global. Moreover, the regional analysis was focused on 9 regions of the planet. Neutral and non-significant DOD trends are recorded over ocean, land and global. In dust affected areas the regional analysis revealed significant DOD trends. More specifically, strong DOD trends were documented in Central (0.0021 yr^{-1}) and East (−0.0018 yr^{-1}) Sahara, Bodélé Depression (−0.0055 yr^{-1}), Mediterranean (−0.0011 yr^{-1}) and Thar Desert (−0.0053 yr^{-1}). In contrast, non-significant regional DOD trends were depicted in Arabian Peninsula and Gobi Desert. On a regional basis, the trend calculations were strongly affected (in terms of sign, magnitude and statistical significance) by the selection of the starting year and the time period.

The ratio between DOD and AOD trend were computed to examine the effect of dust burden to total AOD. DOD variations affects those of AOD over desert areas while in the Mediterranean it is evident a south-to-north gradient following the latitudinal reduction of dust loads towards the northern parts.

The findings of this study highlight the feasibility of MIDAS dataset for detecting dust variations from global to regional scales over long-term period. The high spatiotemporal resolution of MIDAS provides the opportunity to complement and further expand the existing knowledge on this critical aspect yet not well covered in the field of dust research. Likewise, comparing AOD with DOD tendencies reflects the role of mineral particles load variations on those of the total load. The DOD trends results could be incorporated in chemical models, in order to differentiate the various impacts of dust and non-dust particles, and to further improve their calibration and forecast performance. In addition, the high spatial resolution DOD can be collocated much easier with larger grids used in models and to minimize grid size uncertainties in calculated trends by both approaches. At a future step, the role of meteorological variables as well as of other relevant geophysical factors (e.g. soil moisture, vegetation, land coverage) on the configuration of DOD trends will be investigated thoroughly.

Acknowledgments

We acknowledge support of this work by the project "PANhellenic infrastructure for Atmospheric Composition and climatE change" (MIS 5021516) which is implemented under the Action "*Reinforcement of the Research and Innovation Infrastructure*", funded by the Operational Programme "Competitiveness, Entrepreneurship and Innovation" (NSRF 2014-2020) and co-financed by Greece and the European Union (European Regional Development Fund). The MIDAS dataset has been developed in the framework of the DUST-GLASS project (grant no. 749461; European Union's Horizon 2020 Research and Innovation programme under the Marie Skłodowska-Curie Actions. Antonis Gkikas acknowledges support by the Hellenic Foundation for Research and Innovation (H.F.R.I.) under the "2nd Call for H.F.R.I. Research Projects to support Post-Doctoral Researchers" (Project Acronym: ATLANTAS, Project number: 544). Vassilis Amiridis acknowledges support from the European Research Council (grant no. 725698; D-TECT). Stelios Kazadzis acknowledges the International Network to Encourage the Use of Monitoring and Forecasting Dust Products (inDust) COST Action CA16202.

https://doi.org/10.5194/acp-2021-418
Preprint. Discussion started: 28 June 2021

Author contribution

SAL was responsible for the whole analysis and the preparation of the initial manuscript with support from VS. AG processed the MIDAS dataset and had an advisory role in the relevant parts of the study. AK and SK conceptualized the main objective of the manuscript and supervised the progress. VA provided feedback on the scientific discussions. All authors contributed to the revision and the final editing of the initial manuscript.

Competing interests

The authors declare that they have no competing interests.

References

Adesina, A. J., Kumar, K. R., Sivakumar, V. and Piketh, S. J.: Intercomparison and assessment of long-term (2004–2013) multiple satellite aerosol products over two contrasting sites in South Africa, J. Atmos. Solar-Terrestrial Phys., 148, 82–95, https://doi.org/10.1016/j.jastp.2016.09.001, 2016.

Alfaro-Contreras, R., Zhang, J., Reid, J. S. and Christopher, S.: A study of 15-year aerosol optical thickness and direct shortwave aerosol radiative effect trends using MODIS, MISR, CALIOP and CERES, Atmos. Chem. Phys., 17(22), 13849–13868, https://doi.org/10.5194/acp-17-13849-2017, 2017.

Alizadeh-Choobari, O., Zawar-Reza, P., Sturman, A.: The global distribution of mineral dust and its impacts on the climate system: A review, Atmos. Res., 138, 152–165, 1174, https://doi.org/10.1016/j.atmosres.2013.11.007, 2014a.

Alizadeh-Choobari, O., Zawar-Reza, P., Sturman, A.: The “wind of 120 days” and dust storm activity over the Sistan Basin, Atmos. Res., 143, 328–341, https://doi.org/10.1016/j.atmosres.2014.02.001, 2014b.

Alizadeh-Choobari, O., Sturman, A. and Zawar-Reza, P.: A global satellite view of the seasonal distribution of mineral dust and its correlation with atmospheric circulation, Dyn. Atmos. Ocean., 68, 20–34, https://doi.org/10.1016/j.dynatmoce.2014.07.002, 2014c.

Amiridis, V., Wandinger, U., Marinou, E., Giannakaki, E., Tsekeri, A., Basart, S., Kazadzis, S., Gkikas, A., Taylor, M., Baldasano, J., and Ansmann, A.: Optimizing CALIPSO Saharan dust retrievals, Atmos. Chem. Phys., 13, 12089–12106, https://doi.org/10.5194/acp-13-12089-2013, 2013.

https://doi.org/10.5194/acp-2021-418
Preprint. Discussion started: 28 June 2021

Atmospheric Chemistry and Physics Discussions

Amiridis, V., Marinou, E., Tsekeri, A., Wandinger, U., Schwarz, A., Giannakaki, E., Mamouri, R., Kokkalis, P., Binietoglou, I., Solomos, S., Herekakis, T., Kazadzis, S., Gerasopoulos, E., Proestakis, E., Kottas, M., Balis, D., Papayannis, A., Kontoes, C., Kourtidis, K., Papagiannopoulos, N., Mona, L., Pappalardo, G., Le Rille, O., and Ansmann, A.: LIVAS: a 3-D multi-wavelength aerosol/cloud database based on CALIPSO and EARLINET, Atmos. Chem. Phys., 15, 7127–7153, https://doi.org/10.5194/acp15-7127-2015, 2015.

An, L., Che, H., Xue, M., Zhang, T., Wang, H., Wang, Y., Zhou, C., Zhao, H., Gui, K., Zheng, Y., Sun, T., Liang, Y., Sun, E., Zhang, H. and Zhang, X.: Temporal and spatial variations in sand and dust storm events in East Asia from 2007 to 2016: Relationships with surface conditions and climate change, Sci. Total Environ., 633, 452–462, https://doi.org/10.1016/j.scitotenv.2018.03.068, 2018.

Babu, S. S., Manoj, M. R., Moorthy, K. K., Gogoi, M. M., Nair, V. S., Kompalli, S. K., Satheesh, S. K., Niranjan, K., Ramagopal, K., Bhuyan, P. K. and Singh, D.: Trends in aerosol optical depth over Indian region: Potential causes and impact indicators, J. Geophys. Res. Atmos., 118(20), 11,794-11,806, https://doi.org/10.1002/2013JD020507, 2013.

Basart, S., Pérez, C., Cuevas, E., Baldasano, J. M., and Gobbi, G. P.: Aerosol characterization in Northern Africa, Northeastern Atlantic, Mediterranean Basin and Middle East from direct-sun AERONET observations, Atmos. Chem. Phys., 9, 8265–8282, https://doi.org/10.5194/acp-9-8265-2009, 2009.

Che, H., Gui, K., Xia, X., Wang, Y., Holben, B. N., Goloub, P., Cuevas-Agulló, E., Wang, H., Zheng, Y., Zhao, H., and Zhang, X.: Large contribution of meteorological factors to inter-decadal changes in regional aerosol optical depth, Atmos. Chem. Phys., 19, 10497–10523, https://doi.org/10.5194/acp-19-10497-2019, 2019.

Chen, J. L., Pekker, T., Wilson, C. R., Tapley, B. D., Kostianoy, A. G., Cretaux, J. F. and Safarov, E. S.: Long-term Caspian Sea level change, Geophys. Res. Lett., 44(13), 6993–7001, https://doi.org/10.1002/2017GL073958, 2017.

Clarisse, L., Clerbaux, C., Franco, B., Hadji-Lazaro, J., Whitburn, S., Kopp, A. K., Hurtmans, D., and Coheur, P.-F.: A Decadal Data Set of Global Atmospheric Dust Retrieved From IASI Satellite Measurements, J. Geophys. Res.-Atmos., 124, 1618–1647, https://doi.org/10.1029/2018JD029701, 2019.

Dahutia, P., Pathak, B., and Bhuyan, P. K.: Aerosols characteristics, trends and their climatic implications over Northeast India and adjoining South Asia, Int. J. Climatol., 38, 1234–1256, https://doi.org/10.1002/joc.5240, 2017.

de Meij, A., Pozzer, A. and Lelieveld, J.: Trend analysis in aerosol optical depths and pollutant emission estimates between 2000 and 2009, Atmos. Environ., 51, 75–85, https://doi.org/10.1016/j.atmosenv.2012.01.059, 2012.

https://doi.org/10.5194/acp-2021-418
Preprint. Discussion started: 28 June 2021

Atmospheric Chemistry and Physics Discussions

Elguindi, N., Solmon, F., Turuncoglu, U.: Quantifying some of the impacts of dust and other aerosol on the Caspian Sea region using a regional climate model. Clim. Dyn., 46, 41–55, https://doi.org/10.1007/s00382-015-2566-5, 2016.

Evan, A. T., Flamant, C., Gaetani, M., and Guichard, F.: The past, present and future of African dust, Nature, 531, 493–495, https://doi.org/10.1038/nature17149, 2016.

Floutsi, A. A., Korras-Carraca, M. B., Matsoukas, C., Hatzianastassiou, N. and Biskos, G.: Climatology and trends of aerosol optical depth over the Mediterranean basin during the last 12 years (2002-2014) based on Collection 006 MODIS-Aqua data, Sci. Total Environ., 551–552, 292–303, https://doi.org/10.1016/j.scitotenv.2016.01.192, 2016.

Gelaro, R, McCarty, W., Suárez, M. J., Todling, R., Molod, A., Takacs, L., Randles, C. A., Darmenov, A., Bosilovich, M. G., Reichle, R., Wargan, K., Coy, L., Cullather, R., Draper, C., Akella, S., Buchard, V., Conaty, A., da Silva, A. M., Gu, W., Kim, G., Koster, R., Lucchesi, R., Merkova, D., Nielsen, J. E., Partyka, G., Pawson, S., Putman, W., Rienecker, M., Schubert, S. D., Sienkiewicz, M., and Zhao, B.: The Modern-Era Retrospective Analysis for Research and Applications, Version 2 (MERRA-2), J. Climate, 30, 5419–5454, https://doi.org/10.1175/JCLI-D-16-0758.1, 2017.

Ginoux, P., Prospero, J. M., Gill, T. E., Hsu, N. C., and Zhao, M.: Global-scale attribution of anthropogenic and natural dust sources and their emission rates based on MODIS Deep Blue aerosol products, Rev. Geophys., 50, RG3005, https://doi.org/10.1029/2012RG000388, 2012.

Gkikas, A., Houssos, E. E., Lolis, C. J., Bartzokas, A., Mihalopoulos, N., and Hatzianastassiou, N.: Atmospheric circulation evolution related to desert-dust episodes over the Mediterranean, Q. J. Roy. Meteor. Soc., 141, 1634–1645, https://doi.org/10.1002/qj.2466, 2015.

Gkikas, A., Basart, S., Hatzianastassiou, N., Marinou, E., Amiridis, V., Kazadzis, S., Pey, J., Querol, X., Jorba, O., Gassó, S., and Baldasano, J. M.: Mediterranean intense desert dust outbreaks and their vertical structure based on remote sensing data, Atmos. Chem. Phys., 16, 8609–8642, https://doi.org/10.5194/acp-16-8609-2016, 2016.

Gkikas, A., Proestakis, E., Amiridis, V., Kazadzis, S., Di Tomaso, E., Tsekeri, A., Marinou, E., Hatzianastassiou, N., and Pérez García-Pando, C.: ModIs Dust AeroSol (MIDAS): a global fine-resolution dust optical depth data set, Atmos. Meas. Tech., 14, 309–334, https://doi.org/10.5194/amt-14-309-2021, 2021

Gkikas, A., Proestakis, E., Amiridis, V., Kazadzis, S., Di Tomaso, E., Marinou, E., Hatzianastassiou, N., and Pérez García-Pando, C.: Quantification of the dust optical depth across spatiotemporal scales with the MIDAS global dataset (2003-1017), in preparation, 2021.

Gläser, G., Wernli, H., Kerkweg, A., and Teubler, F.: The transatlantic dust transport from North Africa to the Americas-Its characteristics and source regions, J. Geophys. Res.-Atmos., 120, 11231–11252, https://doi.org/10.1002/2015JD023792, 2015.

Goudie, A.S. and Middelton, N.J.: Desert Dust in the Global System, Springer, 2006.

Griffin, D. W., Kellogg, C. A., Garrison, V. H., and Shinn, E. A.: The global transport of dust. An intercontinental river of dust, microorganisms and toxic chemicals flows through the Earth's atmosphere, Am. Sci., 90, 228–235, 2002.

Guo, J., Xu, H., Liu, L., Chen, D., Peng, Y., Yim, S. H. L., Yang, Y., Li, J., Zhao, C., and Zhai, P.: The trend reversal of dust aerosol over East Asia and the North Pacific Ocean attributed to large-scale meteorology, deposition and soil moisture, J. Geophys. Res.-Atmos., 124, 10450–10466, https://doi.org/10.1029/2019JD030654, 2019

Guo, J. P., Zhang, X. Y., Wu, Y. R., Zhaxi, Y., Che, H. Z., La, B., Wang, W. and Li, X. W.: Spatio-temporal variation trends of satellite-based aerosol optical depth in China during 1980-2008, Atmos. Environ., 45(37), 6802–6811, https://doi.org/10.1016/j.atmosenv.2011.03.068, 2011.

Hammer, M. S., Martin, R. V., Li, C., Torres, O., Manning, M., and Boys, B. L.: Insight into global trends in aerosol composition from 2005 to 2015 inferred from the OMI Ultraviolet Aerosol Index, Atmos. Chem. Phys., 18, 8097–8112, https://doi.org/10.5194/acp-18-8097-2018, 2018.

Hsu, N. C., Gautam, R., Sayer, A. M., Bettenhausen, C., Li, C., Jeong, M. J., Tsay, S.-C., and Holben, B. N.: Global and regional trends of aerosol optical depth over land and ocean using SeaWiFS measurements from 1997 to 2010, Atmos. Chem. Phys., 12, 8037–8053, https://doi.org/10.5194/acp-12-8037-2012, 2012.

Hu, K., Kumar, K. R., Kang, N., Boiyo, R. and Wu, J.: Spatiotemporal characteristics of aerosols and their trends over mainland China with the recent Collection 6 MODIS and OMI satellite datasets, Environ. Sci. Pollut. Res., 25(7), 6909–6927, https://doi.org/10.1007/s11356-017-0715-6, 2018.

Huang, J., Zhang, C., and Prospero, J. M.: African dust outbreaks: a satellite perspective of temporal and spatial variability over the tropical Atlantic Ocean, J. Geophys. Res., 115, D05202, https://doi.org/10.1029/2009JD012516, 2010.

Jin, Q. and Wang, C.: The greening of Northwest Indian subcontinent and reduction of dust abundance resulting from Indian summer monsoon revival, Sci. Rep., 8(1), 1–9, https://doi.org/10.1038/s41598-018-23055-5, 2018.

Kalashnikova, O. V. and Kahn, R. A.: Mineral dust plume evolution over the Atlantic from MISR and MODIS aerosol retrievals, J. Geophys. Res., 113, D24204, https://doi.org/10.1029/2008JD010083, 2008.

Klingmüller, K., Pozzer, A., Metzger, S., Stenchikov, G. L. and Lelieveld, J.: Aerosol optical depth trend over the Middle East, Atmos. Chem. Phys., 16(8), 5063–5073, https://doi.org/10.5194/acp-16-5063-2016, 2016.

Kok, J. F., Ridley, D. A., Zhou, Q., Miller, R. L., Zhao, C., Heald, C. L., Ward, D. S., Albani, S., and Haustein, K.: Smaller desert dust cooling effect estimated from analysis of dust size and abundance, Nat. Geosci., 10, 274–278, https://doi.org/10.1038/ngeo2912, 2017.

Kumar, K. R., Yin, Y., Sivakumar, V., Kang, N., Yu, X., Diao, Y., Adesina, A. J. and Reddy, R. R.: Aerosol climatology and discrimination of aerosol types retrieved from MODIS, MISR and OMI over Durban (29.88°S, 31.02°E), South Africa, Atmos. Environ., 117, 9–18, https://doi.org/10.1016/j.atmosenv.2015.06.058, 2015.

Kumar, K. R., Boiyo, R., Madina, A. and Kang, N.: A 13-year climatological study on the variations of aerosol and cloud properties over Kazakhstan from remotely sensed satellite observations, J. Atmos. Solar-Terrestrial Phys., 179, 55–68, https://doi.org/10.1016/j.jastp.2018.06.014, 2018.

Lakshmi, N. B., Babu, S. S. and Nair, V. S.: Recent Regime Shifts in Mineral Dust Trends over South Asia from Long-Term CALIPSO Observations, IEEE Trans. Geosci. Remote Sens., 57(7), 4485–4489, https://doi.org/10.1109/TGRS.2019.2891338, 2019.

Levy, R. C., Leptoukh, G. G., Kahn, R., Zubko, V., Gopalan, A., and Remer, L. A.: A critical look at deriving monthly aerosol optical depth from satellite data, IEEE Transactions on Geoscience and Remote Sensing, 47, 2942–2956, https://doi.org/10.1109/TGRS.2009.2013842, 25, 2009.

Logothetis, S.-A., Salamalikis, V. and Kazantzidis, A.: Aerosol classification in Europe, Middle East, North Africa and Arabian Peninsula based on AERONET Version 3, Atmos. Res., 239, https://doi.org/10.1016/j.atmosres.2020.104893, 2020.

Logothetis, S.-A., Salamalikis, V. and Kazantzidis, A.: The impact of different aerosol properties and types on direct aerosol radiative forcing and efficiency using AERONET version 3, Atmos. Res., 250, https://doi.org/10.1016/j.atmosres.2020.105343, 2021.

Li, J., Carlson, B. E., Dubovik, O. and Lacis, A. A.: Recent trends in aerosol optical properties derived from AERONET measurements, Atmos. Chem. Phys., 14(22), 12271–12289, https://doi.org/10.5194/acp-14-12271-2014, 2014.

https://doi.org/10.5194/acp-2021-418
Preprint. Discussion started: 28 June 2021

Mahowald, N., Albani, S., Kok, J. F., Engelstaeder, S., Scanza, R., Ward, D. S., and Flanner, M. G.: The size distribution of desert dust aerosols and its impact on the Earth system, Aeolian Res., 15, 53–71, https://doi.org/10.1016/j.aeolia.2013.09.002, 2014.

Mona, L., Amodeo, A., Pandolfi, M., and Pappalardo, G.: Saharan dust intrusions in the Mediterranean area: Three years of Raman lidar measurements, J. Geophys. Res., 111, D16203, https://doi.org/10.1029/2005JD006569, 2006.

Mona, L., Liu, Z., Müller, D., Omar, A., Papayannis, A., Pappalardo, G., Sugimoto, N., and Vaughan, M.: Lidar Measurements for Desert Dust Characterization: An Overview, Adv. Meteorol., 2012, 356265, https://doi.org/10.1155/2012/356265, 2012.

Nabat, P., Somot, S., Mallet, M., Chiapello, I., Morcrette, J. J., Solmon, F., Szopa, S., Dulac, F., Collins, W., Ghan, S., Horowitz, L. W., Lamarque, J. F., Lee, Y. H., Naik, V., Nagashima, T., Shindell, D., and Skeie, R.: A 4-D climatology (1979–2009) of the monthly tropospheric aerosol optical depth distribution over the Mediterranean region from a comparative evaluation and blending of remote sensing and model products, Atmos. Meas. Tech., 6, 1287–1314, https://doi.org/10.5194/amt-6-1287-2013, 2013.

Ningombam, S. S., Larson, E. J. L., Dumka, U. C., Estellés, V., Campanelli, M. and Steve, C.: Long-term (1995–2018) aerosol optical depth derived using ground based AERONET and SKYNET measurements from aerosol aged-background sites, Atmos. Pollut. Res., 10(2), 608–620, https://doi.org/10.1016/j.apr.2018.10.008, 2019.

Notaro, M., Yu, Y., and Kalashnikova, O. V.: Regime shift in Arabian dust activity, triggered by persistent Fertile Crescent drought, J. Geophys. Res.-Atmos., 120, 10229–10249, https://doi.org/10.1002/2015JD023855, 2015.

O'Neill, N. T., Ignatov, A., Holben, B. N., and Eck, T. F.: The lognormal distribution as a reference for reporting aerosol optical depth statistics; Empirical tests using multi-year, multi-site AERONET Sunphotometer data, Geophys. Res. Lett., 27, 3333–3336, https://doi.org/10.1029/2000GL011581, 2000.

Papadimas, C. D., Hatzianastassiou, N., Mihalopoulos, N., Querol, X., and Vardavas, I.: Spatial and temporal variability in aerosol properties over the Mediterranean basin based on 6- year (2000–2006) MODIS data, J. Geophys. Res., 113, D11205, https://doi.org/10.1029/2007JD009189, 2008.

Papayannis, A., Amiridis, V., Mona, L., Tsaknakis, G., Balis, D., Bösenberg, J., Chaikovski, A., De Tomasi, F., Grigorov, I., Mattis,I., Mitev, V., Muller, D., Nickovic, S., Pérez, C., Pietruczuk, A., Pisani, G., Ravetta, F., Rizi, V., Sicard, M., Trickl, T., Wiegner, M., Gerding, M., Mamouri, R. E., D'Amico, G., and Pappalardo, G.: Systematic lidar observations of Saharan dust over Europe in the frame of EARLINET (2000–2002), J. Geophys. Res., 113, D10204, https://doi.org/10.1029/2007JD009028, 2008.

Pandey, S. K., Vinoj, V., Landu, K. and Babu, S. S.: Declining pre-monsoon dust loading over South Asia: Signature of a changing regional climate, Sci. Rep., 7(1), 1–10, https://doi.org/10.1038/s41598-017-16338-w, 2017.

Filonchyk, M., Yan, H., Zhang, Z., Yang, S., Li, W. and Li, Y.: Combined use of satellite and surface observations to study aerosol optical depth in different regions of China, Sci. Rep., 9 (1), 1–15, doi:10.1038/s41598-019-42466-6, 2019.

Pozzer, A., de Meij, A., Yoon, J., Tost, H., Georgoulias, A. K., and Astitha, M.: AOD trends during 2001–2010 from observations and model simulations, Atmos. Chem. Phys., 15, 5521–5535, https://doi.org/10.5194/acp-15-5521-2015, 2015.

Proestakis, E., Amiridis, V., Marinou, E., Georgoulias, A. K., Solomos, S., Kazadzis, S., Chimot, J., Che, H., Alexandri, G., Binietoglou, I., Daskalopoulou, V., Kourtidis, K. A., de Leeuw, G., and van der A, R. J.: Nine-year spatial and temporal evolution of desert dust aerosols over South and East Asia as revealed by CALIOP, Atmos. Chem. Phys., 18, 1337-1362, https://doi.org/10.5194/acp-18-1337-2018, 2018.

Prospero, J. M., Ginoux, P., Torres, O., Nicholson, S. E., and Gill, T. E.: Environmental characterization of global sources of atmospheric soil dust identified with the Nimbus 7 Total Ozone Mapping Spectrometer (TOMS) absorbing aerosol product, Rev. Geophys., 40, 2-1–2-31, https://doi.org/10.1029/2000RG000095, 2002.

Prospero, J. M. and Lamb, P. J.: African Droughts and Dust Transport to the Caribbean: Climate Change Implications, Science, 302, 1024–1027, https://doi.org/10.1126/science.1089915, 2003.

Prospero, J. M. and Mayol-Bracero, O. L.: Understanding the transport and impact of African dust on the Caribbean Basin, Bull. Am. Meteorol. Soc., 94(9), 1329–1337, https://doi.org/10.1175/BAMS-D-12-00142.1, 2013.

Rajot, J. L., Formenti, P., Alfaro, S., Desboeufs, K., Chevaillier, S., Chatenet, B., Gaudichet, A., Journet, E., Marticorena, B., Triquet, S., Maman, A., Mouget, N., and Zakou, A.: AMMA dust experiment: An overview of measurements performed during the dry season special observation period (SOP0) at the Banizoumbou (Niger) supersite, J Geophys Res-Atmos, 113, https://doi.org/10.1029/2008JD009906, 2008.

Rashki, A., Kaskaoutis, D. G., Francois, P., Kosmopoulos, P. G. and Legrand, M.: Dust-storm dynamics over Sistan region, Iran: Seasonality, transport characteristics and affected areas, AEOLIAN Res., 16, 35–48, https://doi.org/10.1016/j.aeolia.2014.10.003, 2015.

https://doi.org/10.5194/acp-2021-418
Preprint. Discussion started: 28 June 2021

Remer, L. A., Kleidman, R. G., Levy, R. C., Kaufman, Y. J., Tanré, D., Mattoo, S., Martins, J. V., Ichoku, C., Koren, I., Yu, H., and Holben, B. N.: Global aerosol climatology from the MODIS satellite sensors, J. Geophys. Res.-Atmos., 113, d14S07, https://doi.org/10.1029/2007JD009661, 2008.

Sayer, A. M. and Knobelspiesse, K. D.: How should we aggregate data? Methods accounting for the numerical distributions, with an assessment of aerosol optical depth, Atmos. Chem. Phys., 19, 15023–15048, https://doi.org/10.5194/acp-19-15023-2019, 2019.

Schepanski, K.: Transport of mineral dust and its impact on climate, Geosciences, 8, 151, https://doi.org/10.3390/geosciences8050151, 2018.

Shikwambana, L. and Sivakumar, V.: Global distribution of aerosol optical depth in 2015 using CALIPSO level 3 data, J. Atmos. Solar-Terrestrial Phys., 173, 150–159, https://doi.org/10.1016/j.jastp.2018.04.003, 2018.

Shi, L., Zhang, J., Yao, F., Zhang, D. and Guo, H.: Drivers to dust emissions over dust belt from 1980 to 2018 and their variation in two global warming phases. Sci. Total Environ., 767, 144860, https://doi.org/10.1016/j.scitotenv.2020.144860, 2021.

Song, Q., Zhang, Z., Yu, H., Ginoux, P., and Shen, J.: Global Dust Optical Depth Climatology Derived from CALIOP and MODIS Aerosol Retrievals on Decadal Time Scales: Regional and Interannual Variability, Atmos. Chem. Phys. Discuss. [preprint], https://doi.org/10.5194/acp-2021-1, 17 February 2021.

Textor, C., Schulz, M., Guibert, S., Kinne, S., Balkanski, Y., Bauer, S., Berntsen, T., Berglen, T., Boucher, O., Chin, M., Dentener, F., Diehl, T., Easter, R., Feichter, H., Fillmore, D., Ghan, S., Ginoux, P., Gong, S., Grini, A., Hendricks, J., Horowitz, L., Huang, P., Isaksen, I., Iversen, I., Kloster, S., Koch, D., Kirkevåg, A., Kristjansson, J. E., Krol, M., Lauer, A., Lamarque, J. F., Liu, X., Montanaro, V., Myhre, G., Penner, J., Pitari, G., Reddy, S., Seland, Ø., Stier, P., Takemura, T., and Tie, X.: Analysis and quantification of the diversities of aerosol life cycles within AeroCom, Atmos. Chem. Phys., 6, 1777–1813, https://doi.org/10.5194/acp-6-1777-2006, 2006.

Todd, M.C., Washington, R., Martins, J.V., Dubovik, O., Lizcano, G., M'Bainayel, S., Engelstaedter, S.: Mineral dust emission from the Bodélé Depression nothern Chad, during BoDEx 2005, J. Geophys. Res. Atmos., 112, 1–12, https://doi.org/10.1029/2006JD007170, 2007.

Torres, O., Bhartia, P. K., Herman, J. R., Sinyuk, A., Ginoux, P., and Holben, B.: A long-term record of aerosol optical depth from TOMS observations and comparison to AERONET measurements, J. Atmos. Sci., 59, 398–413, https://doi.org/10.1175/1520- 0469(2002)0592.0.CO;2, 2002.

Tsamalis, C., Chédin, A., Pelon, J., and Capelle, V.: The seasonal vertical distribution of the Saharan Air Layer and its modulation by the wind, Atmos. Chem. Phys., 13, 11235–11257, https://doi.org/10.5194/acp-13-11235-2013, 2013.

Voss, K. K., and Evan, A. T.: A new satellite-based global climatology of dust aerosol optical depth, Journal of Applied Meteorology and Climatology, https://doi.org/10.1175/JAMC-D-19-0194.1, 2020.

Washington, R., Todd, M.C., Engelstaedter, S., Mbainayel, S., Mitchell, F.: Dust and the low-level circulation over the Bodélé Depression, Chad: Observations from BoDEx 2005, J. Geophys. Res. Atmos., 111, 1–15, https://doi.org/10.1029/2005JD006502, 2006.

Weatherhead, E. C., Reinsel, G. C., Tiao, G. C., Meng, X.-L., Choi, D., Cheang, W.-K., Keller, T., DeLuisi, J., Wuebbles, D. J., Kerr, J. B., Miller, A. J., Oltmans, S. J., and Frederick, J. E.: Factors affecting the detection of trends: Statistical considerations and applications to environmental data, J. Geophys. Res., 103(D14), 17149–17161, https://doi.org/10.1029/98JD00995,1998.

van der Does, M., Knippertz, P., Zschenderlein, P., Harrison, R. G., and Stuut, J. B. W.: The mysterious long-range transport of giant mineral dust particles, Sci. Adv., 4, eaau2768, https://doi.org/10.1126/sciadv.aau2768, 2018.

Wei, J., Peng, Y., Mahmood, R., Sun, L., and Guo, J.: Intercomparison in spatial distributions and temporal trends derived from multi-source satellite aerosol products, Atmos. Chem. Phys., 19, 7183–7207, https://doi.org/10.5194/acp-19-7183-2019, 2019.

Xi, X. and Sokolik, I. N.: Dust interannual variability and trend in Central Asia from 2000 to 2014 and their climatic linkages, J. Geophys. Res., 120, 12175–12197, https://doi.org/10.1002/2015JD024092, 2015.

Xian, P., Klotzbach, P. J., Dunion, J. P., Janiga, M. A., Reid, J. S., Colarco, P. R., and Kipling, Z.: Revisiting the relationship between Atlantic dust and tropical cyclone activity using aerosol optical depth reanalyses: 2003–2018, Atmos. Chem. Phys., 20, 15357–15378, https://doi.org/10.5194/acp-20-15357-2020, 2020.

https://doi.org/10.5194/acp-2021-418
Preprint. Discussion started: 28 June 2021

Atmospheric Chemistry and Physics
Open Access
Discussions

Yoon, J., Burrows, J. P., Vountas, M., von Hoyningen-Huene, W., Chang, D. Y., Richter, A., and Hilboll, A.: Changes in atmospheric aerosol loading retrieved from space-based measurements during the past decade, Atmos. Chem. Phys., 14, 6881–6902, https://doi.org/10.5194/acp-14-6881-2014, 2014.

Yu, Y., Notaro, M., Liu, Z., Wang, F., Alkolibi, F., Fadda, E., and Bakhrjy, F.: Climatic controls on the interannual to decadal variability in Saudi Arabian dust activity: Toward the development of a seasonal dust prediction model, J. Geophys. Res.-Atmos., 120, 1739–1758, https://doi.org/10.1002/2014JD022611, 2015.

Yu, H., Tan, Q., Chin, M., Remer, L. A., Kahn, R. A., Bian, H., Kim, D., Zhang, Z., Yuan, T., Omar, A. H., Winker, D. M., Levy, R. C., Kalashnikova, O., Crepeau, L., Capelle, V., and Chedin, A.: Estimates of African dust deposition along the trans-Atlantic transit using the decade-long record of aerosol measurements from CALIOP, MODIS, MISR, and IASI, J. Geophys. Res.-Atmos., 124, 7975–7996, https://doi.org/10.1029/2019JD030574, 2019.

Zender, C. S., Miller, R., and Tegen, I.: Quantifying mineral dust mass budgets: Terminology, constraints, and current estimates, Eos, Transactions American Geophysical Union, 85, 509–512, https://doi.org/10.1029/2004EO480002, 2004.

Zhang, J. and Reid, J. S.: A decadal regional and global trend analysis of the aerosol optical depth using a data-assimilation grade over-water MODIS and Level 2 MISR aerosol products, Atmos. Chem. Phys., 10, 10949–10963, https://doi.org/10.5194/acp-10-10949-2010, 2010.

Zhang, M., Wang, Y., Ma, Y., Wang, L., Gong, W. and Liu, B.: Spatial distribution and temporal variation of aerosol optical depth and radiative effect in South China and its adjacent area, Atmos. Environ., 188, 120–128, https://doi.org/10.1016/j.atmosenv.2018.06.028, 2018.

Zhao, B., Jiang, J. H., Gu, Y., Diner, D., Worden, J., Liou, K. N., Su, H., Xing, J., Garay, M., and Huang, L.: Decadal-scale trends in regional aerosol particle properties and their linkage to emission changes, Environ. Res. Lett, 12, 054021, https://doi.org/10.1088/1748-9326/aa6cb2, 2017.